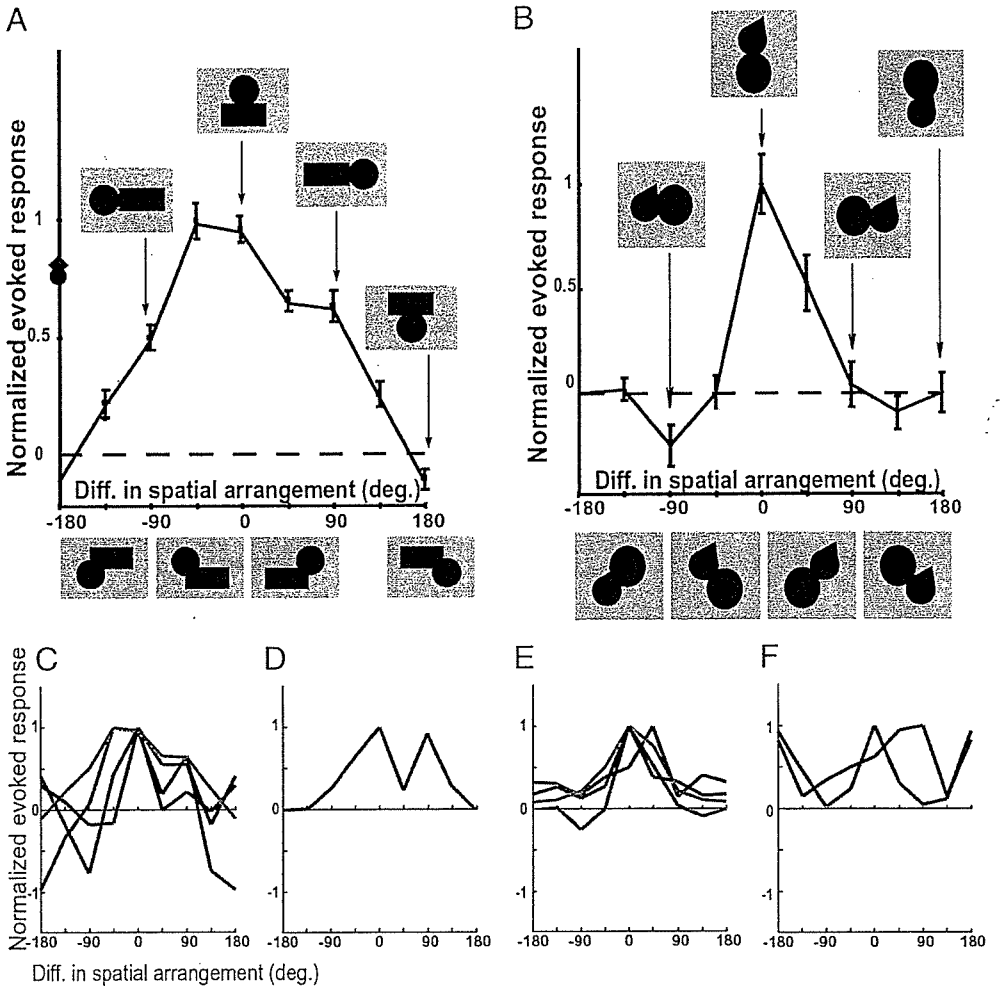


FIG. 9. Selectivity of cells in SRR spots to different spatial arrangements of the upper and the lower parts of their critical features. Normalized responses of the representative cells in Fig. 6, *A* and *B*, are represented in *A* and *B*, respectively. The stimuli were generated from the critical feature of each cell instead of the best object stimulus. Other conventions are the same as those in Fig. 6. One-way ANOVA confirmed that the evoked responses significantly differed depending on the spatial arrangement of the parts ($P < 0.05$). Normalized responses to the critical feature presented at different retinotopic positions are indicated by symbols along the vertical axis in *A*. The distance between the leftmost (●) and rightmost (◆) stimuli was 12.8° (*C–F*). Tuning curves for other cells with single (*C* and *E*) and multiple peaks (*D* and *F*) in spots A (*C* and *D*) and B (*E* and *F*).

arranged in specific spatial relationship (Figs. 6 and 9). In addition, our data show that cells in these spots are less sensitive to changes in visual attributes that are essential to characterize local features, such as color, texture, and local shape: *1*) activity spots showed the same response selectivity for stimulus sets derived from different object images (Fig. 4, *C* and *D*), *2*) neurons in these spots responded equally well to the stimuli including different colors, textures, and local shapes (Fig. 5), and *3*) the critical features of these neurons did not include particular local features (Fig. 7, *B* and *D;* see also Fig. 2). These two sets of results suggest that neurons in these spots were activated when arbitrary local features were arranged in a particular spatial configuration. Further evidence supporting this view is provided by direct comparison between responses to variations in color, texture, and local shape of parts and those to variations in the spatial arrangements of parts: the cells in SRR spots were more selective to particular spatial arrangements of parts than to examined variations in color, texture, and shape (Fig. 10). Therefore in terms of representation of object images, the neurons characterized in this study could play a role in specifying spatial relationships between parts. Altogether we found only four SRR spots among 26 activity spots elicited by "original" object images (16.7%). This relatively small proportion indicates that an object image consists of multiple local features and different types of spatial configurations. In the present study, we only investigated neural representation of one particular type of spatial configuration: two parts aligned vertically. It should be noted that these spots did not respond to the combination of parts when the upper part was rotated 180° (Figs. 6, *C* and *D*, and 9, *C* and *E*), indicating that these neurons are capable of differentiating two parts. Sensitivity of the cells to some unidentified local cues could be essential for differentiating two parts. Further investigations will be necessary to fully understand the neural representation of spatial relationships among parts or local features in general.

Multiple studies with anesthetized as well as alert monkeys have shown that on average, cells in area TE have large receptive fields (Ito et al. 1995; Kobatake and Tanaka 1994; Op De Beeck and Vogels 2000). However, some reports shows that the size of receptive fields of IT cells could be a small portion of the visual field (DiCarlo and Maunsell 2002; also see Op De Beeck and Vogels 2000). Thus one may consider that the sensitivity to a particular spatial arrangement of parts (Figs. 6, 9, and 10) is simply due to upper parts of stimuli falling out of the receptive fields when upper parts were rotated relative to lower parts. One determining factor of receptive field size is the size of stimuli used in these investigations; it has been reported that the size of receptive fields increases when the size of stimuli increases (Ito et al. 1995; Op De Beeck and Vogels 2000). DiCarlo and Maunsell (2002) used stimuli as small as 0.6° but Kobatake and Tanaka (1994) used the stimuli as large as 10°. In the present study, we hand-plotted a receptive field for each cell; on average, receptive fields were as large as 42 × 46°. The stimulus size in our study was 13.3 × 10.9° on

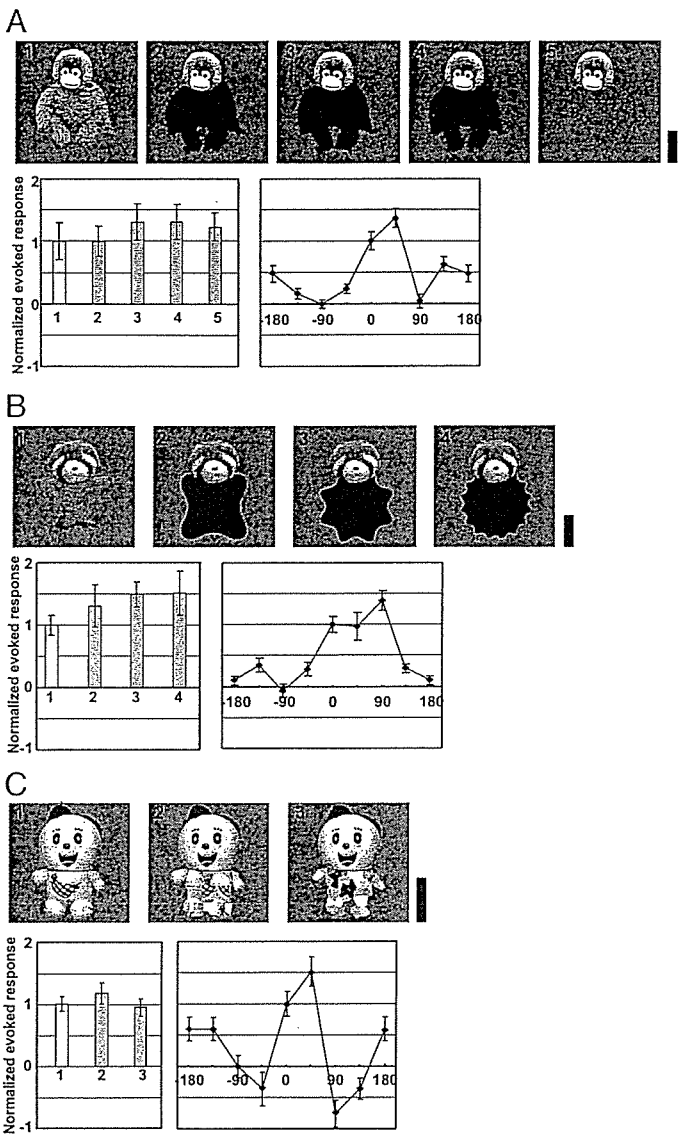


FIG. 10. Tuning specificity of representative neurons to stimuli in which lower parts were filled with different colors (*A*), had different shapes (*B*) or had altered textures (*C*). *A*: tuning specificity for color was examined for red (17.6, 0.506, 0.366), blue (11.7, 0.187, 0.213), green (19.3, 0.278, 0.518), and yellow (32.5, 0.399, 0.491). *Top*: [the numbers in the parentheses give the values for luminance (*Y*), and chromaticity coordinate (*x*, *y*) in CIE color space]. Among 10 cells (6 and 4 cells tested on changes to the *bottom* and *top*, respectively), no cell showed evoked responses that significantly depended on different colors, except for 3 cells tested on changes to the *top* (1-way ANOVA, $P > 0.1$). *B*: tuning specificity for shape was examined with Fourier descriptor stimuli (frequency, 4, 8, and 16; amplitude, 0.8) (*top*). Among 5 cells (4 and 1 cells tested on changes to the *bottom* and *top*, respectively), no cell showed evoked responses that significantly depended on shape (1-way ANOVA, $P > 0.1$). *C*: tuning specificity for texture was examined using stimuli in which the texture within one of the parts was modified. To create coarse texture modification, we partitioned either part of the stimulus into nine rectangular regions and shuffled them (stimulus 2). To create fine texture modification, we first made a Voronoi diagram based on randomly chosen pixels that were at most separated by 1.1° of visual angle. Then each area of the Voronoi region was filled with the color of the pixel which was its own base point (stimulus 3). Among 8 cells (5 and 3 cells tested on modifications to the *bottom* and *top*, respectively), only 2 cells showed evoked responses that significantly depended on differences in texture in either part (1-way ANOVA, $P > 0.1$). *A—C*, recorded from different neurons. In all figures, upper panel shows the stimuli, the *bottom left panel* shows evoked responses to these stimuli normalized to the responses elicited by the original best object image and *bottom right*: the tuning specificity of the same neuron to different spatial arrangements of parts of the best object for that cell. All of these cells were sensitive to particular spatial arrangements of parts. Scale bar, 5°.

average. Thus it is less possible that our results (Figs. 6, 9, and 10) are due to a decrease of responses when the stimuli fell out of the small receptive field, although quantitative analysis of the receptive field for neurons in SRR spots would be necessary in the future.

Finally, although it has been reported that many neurons in area TE respond to visual features less complex than natural objects, it has remained unclear whether these features are related to local features of object images or to more global features (Fujita 1993; Fujita et al. 1992; Ito et al. 1995; Kobatake and Tanaka 1994; Tanaka et al. 1991). Here, by global features we mean the combination of elementary components such as combinations of color and shape and local features. In particular, specification of spatial relationship among parts is one such global features. One important contribution of the present study is that it provides concrete evidence that critical features can be such global features of object images.

## ACKNOWLEDGMENTS

We thank Dr. Etsuro Ito for providing an opportunity for Y. Yamane to conduct this study and for continuous encouragement throughout the study. The authors thank Drs. Kathleen Rockland, Uma R. Maheswari, and Bonnie Lee La Madeleine for helpful comments on an earlier version of the manuscript. We also thank Dr. Ryota Homma for technical support and suggestions.

## GRANTS

This work was partly supported by Research Fellowships of the Japan Society for the Promotion of Young Scientists to Y. Yamane.

## REFERENCES

**Arieli A, Grinvald A, and Slovin H.** Dural substitute for long-term imaging of cortical activity in behaving monkeys and its clinical implications. *J Neurosci Methods* 114: 119–133, 2002.

**Biederman I.** Recognition-by-components: a theory of human image understanding. *Psychol Rev* 94: 115–147, 1987.

**Brincat SL and Connor CE.** Underlying principles of visual shape selectivity in posterior inferotemporal cortex. *Nat Neurosci* 7: 880–886, 2004.

**Bruce C, Desimone R, and Gross CG.** Visual properties of neurons in a polysensory area in superior temporal sulcus of the macaque. *J Neurophysiol* 46: 369–384, 1981.

**Desimone R, Albright TD, Gross CG, and Bruce C.** Stimulus-selective properties of inferior temporal neurons in the macaque. *J Neurosci* 4: 2051–2062, 1984.

**DiCarlo JJ and Maunsell JHR.** Anterior inferotemporal neurons of monkeys engaged in object recognition can be highly sensitive to object retinal position. *J Neurophysiol* 89: 3264–3278, 2002.

**Fujita I.** Columns in the inferotemporal cortex: machinery for visual representation of objects. *Biomed Res* 14: 21, 1993.

**Fujita I, Tanaka K, Ito M, and Cheng K.** Columns for visual features of objects in monkey inferotemporal cortex. *Nature* 360: 343–346, 1992.

**Gochin PM, Miller EK, Gross CG, and Gerstein GL.** Functional interactions among neurons in inferior temporal cortex of the awake macaque. *Exp Brain Res* 84: 505–516, 1991.

**Gross CG.** How inferior temporal cortex became a visual area. *Cereb Cortex* 5: 455–469, 1994.

**Gross CG, Bender DB, and Rocha-Miranda CE.** Visual receptive fields of neurons in inferotemporal cortex of the monkey. *Science* 166: 1303–1306, 1969.

**Gross CG, Bender DB, and Gerstein GL.** Activity of inferior temporal neurons in behaving monkeys. *Neuropsychology* 17: 215–229, 1979.

**Ito M, Tamura H, Fujita I, and Tanaka K.** Size and position invariance of neuronal responses in monkey inferotemporal cortex. *J Neurophysiol* 73: 218–226, 1995.

**Kobatake E and Tanaka K.** Neuronal selectivities to complex object features in the ventral visual pathway of the macaque cerebral cortex. *J Neurophysiol* 71: 856–867, 1994.

**Logothetis NK and Sheinberg DL.** Visual object recognition. *Annu Rev Neurosci* 19: 577–621, 1996.

**Marr D and Nishihara HK.** Representation and recognition of the spatial organization of three-dimensional shapes. *Proc R Soc Lond B Biol Sci* 200: 269–294, 1978.

**Op De Beeck H and Vogels R.** Spatial sensitivity of macaque inferior temporal neurons. *J Comp Neurol* 426: 505–518, 2000.

**Perrett DI, Rolls ET, and Caan W.** Visual neurones responsive to faces in the monkey temporal cortex. *Exp Brain Res* 47: 329–342, 1982.

**Schwartz EL, Desimone R, Albright TD, and Gross CG.** Shape recognition and inferior temporal neurons. *Proc Natl Acad Sci USA* 80: 5776–5778, 1983.

**Tanaka K, Saito H, Fukada Y, and Moriya M.** Coding visual images of objects in the inferotemporal cortex of the macaque monkey. *J Neurophysiol* 66: 170–189, 1991.

**Tsunoda K, Yamane Y, Nishizaki M, and Tanifuji M.** Complex objects are represented in macaque inferotemporal cortex by the combination of feature columns. *Nat Neurosci* 4: 832–838, 2001.

**Wang G, Tanaka K, and Tanifuji M.** Optical imaging of functional organization in the monkey inferotemporal cortex. *Science* 272: 1665–1668, 1996.

**Wang G, Tanifuji M, and Tanaka K.** Functional architecture in monkey inferotemporal cortex revealed by in vivo optical imaging. *Neurosci Res* 32: 33–46, 1998.

**Zahn CT and Roskies RZL.** Fourier descriptors for plane closed curves. *IEEE Trans Comput* 21: 269–281, 1972.

# 深さ方向の内因性イメージング
## ―機能的オプティカルコヒーレンストモグラフィー

ラジャゴパラン　ウママヘスワリ
Rajagopalan　Uma Maheswari
脳統合機能研究チーム理化学研究所（〒351-0198 埼玉県和光市広沢2-1）
Email : uma@brain.riken.jp

### 実験のコツと注意点

内因性信号のイメージングにより神経活動をイメージングできるが[1,2]，その画像は組織内の信号を深さ方向に積分したものになっている．次の点に注意すると，内因性信号を深さ方向に分解して神経活動の断層像を得ることが出来る．1．内因性信号に含まれる光散乱強度変化に敏感なOCT（オプティカルコヒーレンストモグラフィー）を用いて異なる深さでの反射率を計測する．2．OCTは対象となる組織の動きに敏感なので，呼吸などによる動きの補正が必要である．3．脳表面の動きを押さえるために脳表面のアガローズによる固定が欠かせない．4．空気伝搬中における水分子による散乱ノイズを少なくするために光学系全体を窒素でパージすると良い．内因性信号自体が神経活動の伴うものであり，データ解釈する際に注意する必要がある．

## はじめに

光を用いる脳機能観測は非侵襲計測を可能にする有力な手段であると同時に活動を空間パターンとして捕えることができるという利点を持つ．脳研究では，特に機能を空間パターンとして捕えられる点に重点がある．高次神経系において，①多くの場合似たような反応性を持つ神経細胞がクラスターを作っていて，②そのクラスターが意味をもって配列されているため，情報の脳内表現という脳科学の基本的な問題を機能の空間パターンを通して論議できるからである．このような脳機能の光計測技術として，我々の研究室では内因性信号とその延長として光コヒーレンス・トモグラフィ技術[3]（OCT）を用いて脳研究を行っている．

近年，光を用いる方法としてもっとも有利な技術としては内因性信号のイメージング（ISI : Intrinsic Signal Imaging）がある[1,2]．この方法では骨を除去した脳表面を可視光で照明し，脳表面からの反射光をCCDカメラなどで取り込む[4]．視覚刺激や聴覚刺激などによる神経活動に伴う反射光強度の変化が内因性信号と呼ばれている．この方法を用いることにより，脳の活動を空間的なパターンとして得ることができ，様々な脳機能がわかるようになってきた[5]．しかしながら，ISIでは反射強度が深さ方向に積分されているため，特定な深さからの情報を分離するのは不可能である．一方，脳の視覚情報処理を行っている第一次視覚野は六つの層から成り，層によってその特性は異なっている．例えば，第1層には神経細胞が少なく，第2～3層の神経細胞は特定の傾きの格子に反応するが，第4層の細胞はそのような特性を持たない[6]．ISIではこれらの層からの平均された情報しか得られない．さらに，可視光を使うため光が届く深さが数百ミクロンに制限される．

我々は従来のISIの欠点の解決策として機能的光コヒーレンス・トモグラフィ技術（functional OCT）を提案し，神経活動に伴うOCT信号変化を検出するこ

1344-0128/06/¥100/頁/JCLS

とに成功した[5,6]．第2節でOCTの原理と動物への刺激などの生物学的な実験手法と手続きについて説明を行う．第3節では機能OCTイメージングで得られた断層像の結果とその有効性を示すために得られた電気生理学による比較結果について説明する．最後に本技術の展望を述べる．

## fOCT実験

### 1. OCTの原理

OCTの基本原理[3]を図1Aに示す干渉計を用いて説明する．光源からの光はビームスプリッターで2つの光束に分けられる．一方の光束で参照ミラーを照明し，他方の光束は物体を照明する．参照ミラーは一定の速度で移動できるようにしてある．ビームスプリッターから参照ミラー間および物体間の光路長をそれぞれLr，Lsとする．干渉信号は物体光と参照光の光路差がコヒーレンス長内のときにのみ得られる．つまり，干渉信号は二つの光波間で時間的に相関をもっている時にしか得られない．相関長は光源で決まり一般的にはコヒーレンス長（$\Delta\lambda/\lambda_0^2$）で定量化されている．したがって，参照ミラーを移動させ参照面までの光路長を変えることにより，物体内部の任意の位置からの反射光を干渉信号として検出することができる．本実験では低コヒーレンス光源（AFC, Canada）の中心波長（$\lambda_0$）は1.31 $\mu$m，半値幅（$\Delta\lambda$）は50 nm用いた．実験系は単一モード光ファイバーを利用したMach-Zehnder型干渉計である[6]（図1B）．物体である大脳皮質の照明に用いるプローブユニットにはビームを脳表面に対して平行に走査するため，ガルバノミラーが用いられている（図1C）．さらに，CCDカメラが設

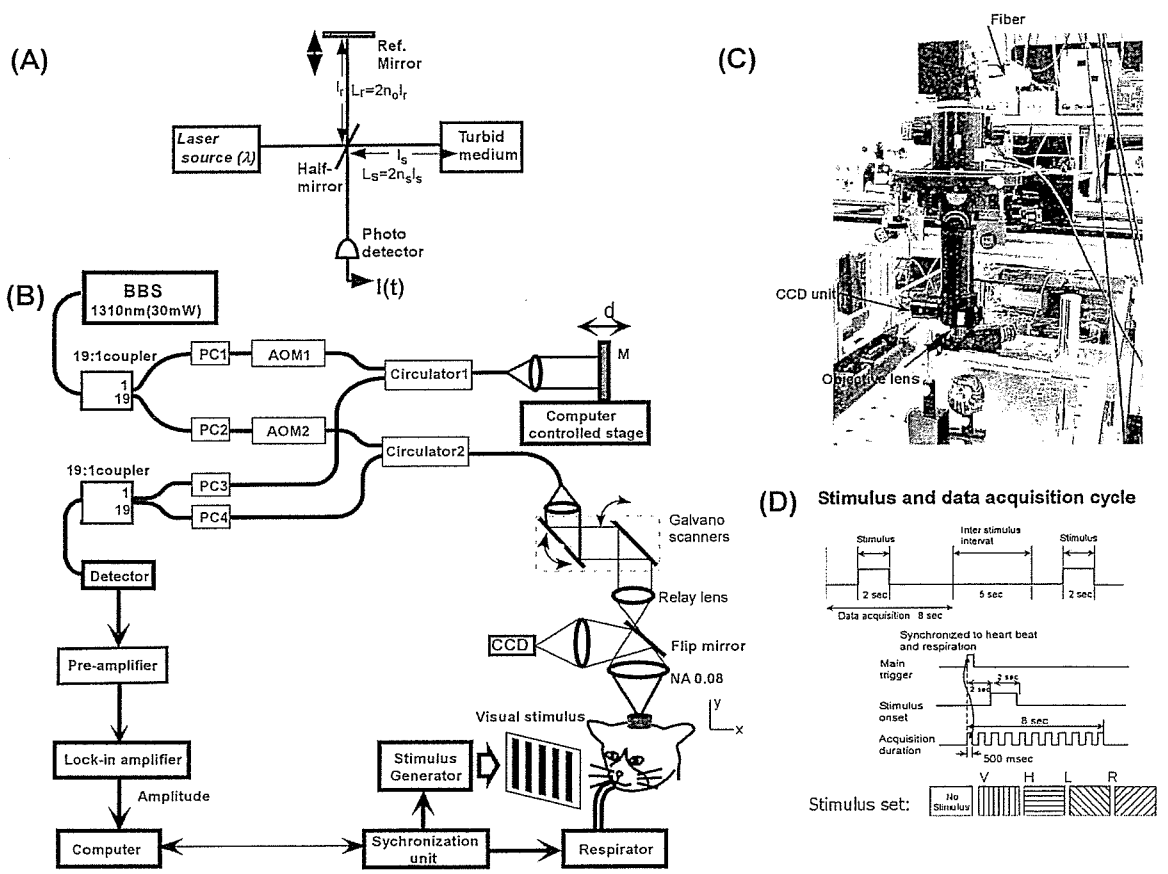


図1　OCTの原理を説明するMichelson型干渉計（A）とネコの第一視覚野からの機能OCT信号計測用Mach-Zehnder heterodyne干渉計の実験系と（B）プローブ部分の写真（C）と視覚刺激とデータ取り込みのタイミング（D）

ここで，BBS：広帯域光源 Broad Band Source，AOM：音響光学変調器 Acousto Optic Modulator，PC：偏光コントローラ Polarization Controller，M：ミラー Mirror，O：対物レンズ Objective lens である．

置されており照射ビームの脳表面上での位置がわかるようにしてある．対物レンズはNA0.08でありビーム直径は19 $\mu$mである．

**2. 生物学実験操作手順**

実験は麻酔下のネコに行った．視覚刺激はVSG2/3の画像ボードにより作成した．刺激には，移動速度は4 °/sで動く空間周波数0.5 cycle/degreeの格子パターン（明部＝8 cd/m$^2$, 暗部＝0 cd/m$^2$）を用いた．刺激セットはコントロール（刺激なし），格子パターン横（0°），縦（90°），45°および135°方向の縞パターンから成る．これらのパターンはランダムな順序で表示される．

実験では5つの視覚刺激からなる刺激セットを全部で40回くり返した．一つの試行は8秒間から成り，その間に参照ミラーとガルバノミラーを走査し，OCT信号を記録する．すべてのデータ取り込みは呼吸と心拍に同期させて行った．視覚刺激とデータ取り込みのタイミングを図1Dに示す．

## fOCT実験と結果

**1. OCT断層画像**

参照ミラーを走査することによって深さ位置dの反射強度分布とそれに加えて，ガルバノミラーによって脳表面上の光の照射位置xを変えることによって*x-d*のOCT反射強度分布を得ることができる（**図2左**）．反射光強度分布（**図2右**）を見ると，ゆっくりした成分上に多くの小さなピークを持つ変調成分があることがわかる．これらは実際に存在する内部の構造によるもので，おそらく層内の異なる細胞や毛細血管などによる屈折率分布を反映している．

**2. OCTによる機能イメージング**

OCTによる機能イメージングを行う前に，内因性信号のイメージング（波長－607 nm）を行った．内因性信号のイメージングから得られた脳表面上での方位選択性のカラムパターンを**図3（左上）**に示す．暗部および明部はそれぞれ0°（横），90°（縦）の格子に反応する領域である．次に，緑線で示された部位からOCTによる機能計測を行った．

計測された光反射率について，刺激前後でのx-d走査結果の比率を格子パターンとコントロールに対して計算する：

$$\gamma_s(x,d,t)=\frac{R_s^{post}(x,d,t)}{\sum_{prescans}R_s^{pre}(x,d,t)} \qquad (1)$$

ここでは，時間tと刺激sに対して得られる光反射率をRs（x, d, t）とした．式（1）により，刺激前後で共通の内部構造による信号が除去され，視覚刺激に対する変化だけが抽出される．ここで，式（1）による計算を行う前に，走査の中で任意のひとつを選び，それ以外の走査の光反射率分布との間で相関関数を求める．相関ピークの位置から走査開始位置のわずかなずれを補正する．

次に，$\gamma_s(x,d,t)$を刺激後1秒から3.5秒について時

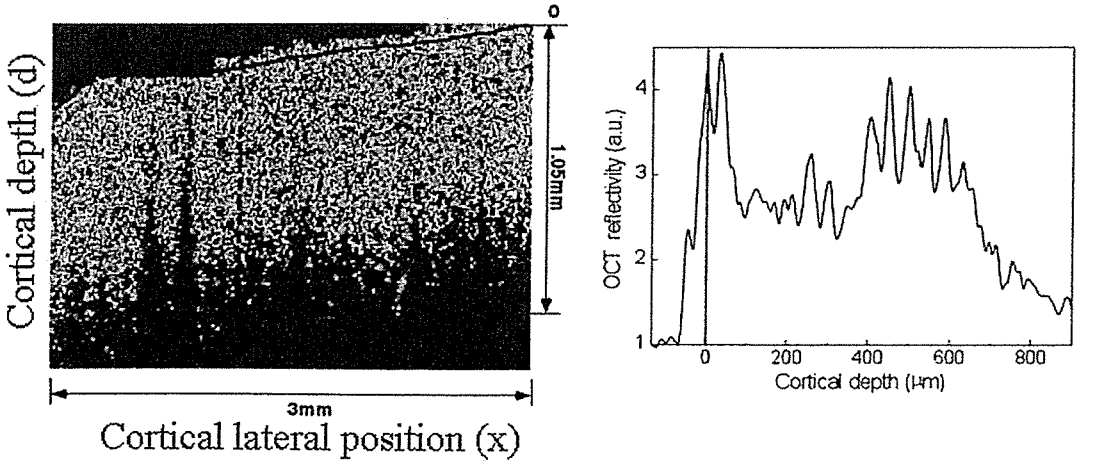


図2　OCTで得られたx-d反射率分布（左）と黒波線部での反射率の深さ分布（右）

(p.14カラー図参照)

間平均する．この時間に内因性信号が最大になることが知られている．個々の格子刺激に対する機能OCT信号は時間平均した$<\gamma_s(x,d)>$を使って，次の式によって定義される：

$$<\gamma_{diff}(x,d)>=<\gamma_{grating}(x,d)>-<\gamma_{control}(x,d)> \quad (2)$$

その結果を図3（下）に示す．

赤と青の領域はそれぞれ横縞と縦縞に反応する部位である．まず，比較的表面に近いつまり浅い領域にはあまり反応が見られなかった．刺激に選択的な信号は100ミクロン以上の深い部位に見られる．これまでカラムは深さ方向では一様だと考えられてきた．しかし機能OCTにより深さ方向に機能的なサブ構造がある可能性を本実験結果は示唆している．深部で見られる刺激選択的な信号はx軸方向には一様ではなく，x軸上の位置によって異なる選択性を示した．この結果の信頼性を調べるために内因性信号との比較を行った．まず，OCTによって得られた反射率分布を反射率を深さ方向に積分した．積分された反射率からx軸に沿った機能信号を計算した．

### 3. 機能OCT信号の起源

図3（右上）は，機能OCT結果（赤線）と内因性信号の空間プロファイル（緑線）をxの関数として重ねて表したものである．機能OCT信号と内因性信号は良く一致した．そこで，機能OCTで得られる信号の起源について検討が必要である．機能OCT信号は散乱強度変化であり神経活動そのものではない．神経活動は以下の生理的な変化を伴う：

1. 血液の体積変化に伴う毛細血管の拡張や収縮などの構造変化
2. 血流変化に伴う赤血球の密度や濃度の変化
3. 神経細胞やグリア細胞の体積変化

これらの変化は散乱強度変化を引き起こす．OCTで得られる反射率はこれらの散乱変化特性により変化する．したがって，図3（下）に示した空間的な信号の局在が神経活動そのものの局在であるか，あるいは，

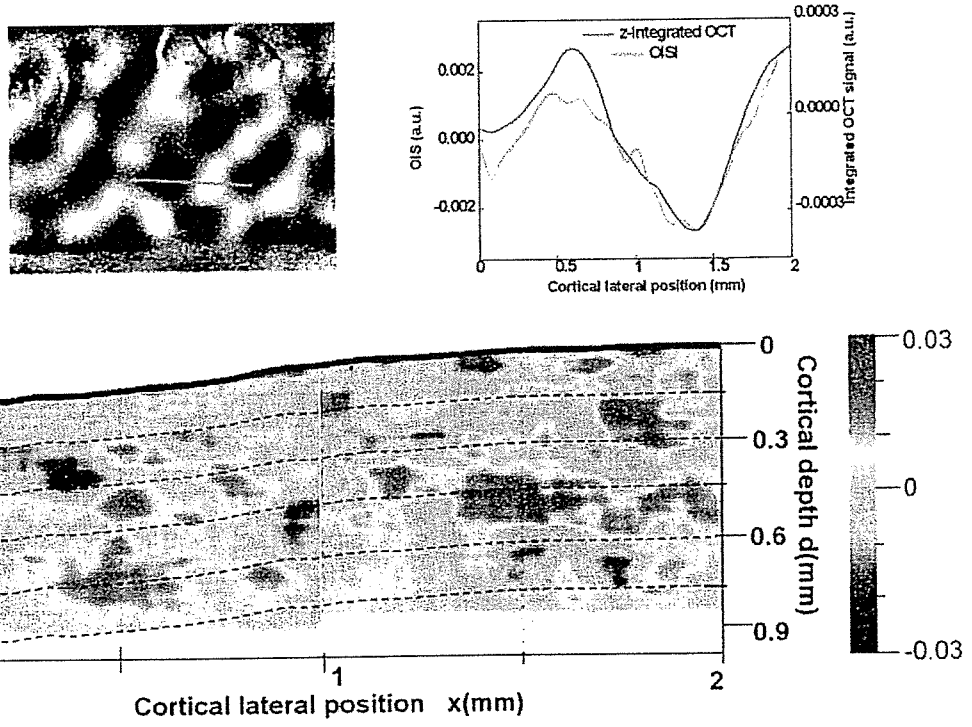


図3　内因性信号マップ（左上）の緑線部で機能OCT(x-d)観測を行った結果を（下）に示す

内因性信号マップでは暗部と明部で示された領域はそれぞれ横縞と縦縞に強く反応する部分である．（右上）内因性信号の黒線部での1次元分布（緑線）と機能OCTマップの積分により得られた結果（赤線）の比較．ここで，積分は深さ方向に分解された反射率をd方向に積分し1次元の機能信号を計算した．

(p.14カラー図参照)

表1

（A）活動電位差から得られる電位差の分布とそれに対応する機能的ＯＣＴマップの強度分布との相関を計算した結果．
（B）三匹の猫から得られた相関結果．

(A)

**Correlation between fOCT and unit profiles**

| Site # | Correlation coeff. for 0-90 deg | Correlation coeff. for 45-135 |
|---|---|---|
| #1 | 0.94 | 0.66 |
| #2 | 0.809 | 0.764 |
| #3 | 0.908 | 0.926 |
| #4 | 0.852 | 0.899 |
| #5 | 0.348 | 0.374 |
| #6 | 0.751 | 0.365 |

(B)

| Cat # | # of sites that show significant correlation ($p<0.005$) |
|---|---|
| **C-22** | 4/8 |
| **C-30** | 9/11 |
| **C-36** | 5/11 |

神経活動に起因する散乱強度変化を引き起こすメカニズムに空間的な局在があることも考えられる．したがって，機能的OCTによって得られる信号の起源を明らかにすることが重要である．

### 4. 電気生理実験との比較

次に，起源を明らかにするために電気生理実験を行った．不連続的に得られた活動電位と機能的OCTで得られる深さ応答信号を比較した．比較の精度を上げるためｘ軸方向に垂直なｙ軸方向にも比較的狭い領域で走査を行い，ｙ方向に積分された機能OCTマップを用いた．活動電位差から得られる電位差の分布とそれに対応する機能的OCTマップの強度分布との相関を計算した結果を（表1A）に示す．表から電極位置6箇所の内4箇所において高い相関が得られていることがわかる．さらに，三匹の猫から得られた統計的に高い相関値結果を（表1B）に示す．これらの結果から機能的OCTで得られる信号は神経活動を反映していると言える．つまり神経活動が空間的に局在していると結論することができる．

## まとめ

我々の機能OCTシステムは理論上30 $\mu$mまでの機能構造を深さ方向に分解できる能力を持っている．分解能は光源のコヒーレンス長で決まるのでより短いコヒーレンス長を持つ光源を使用することにより，さらに分解能の改善が可能である．

我々が提案した機能OCT技術は脳の機能研究の手法において活動電位記録と内因性信号イメージングとを補足するものである．活動電位記録は一点での測定技術であり単一の神経細胞を調べるため深さ方面には不連続にしか測定できない．その反面，内因性信号は多くの細胞集団活動をミクロンレベルで計測できるが深さでは分解できない．これらの従来技術に対して，本技術では深さ情報を分解可能であり，３次元空間でミクロンレベルの分解能を持つ非常に優れた技術である．

### 参考文献


1) 福田光洋：内因性信号の起源とそれを使った機能構造の可視化．脳21 8：443-447, 2005.
2) 角田和繁：網膜における内因性信号．脳21 9：88-92, 2006.
3) Bouma BE, Tearney GJ : Handbook of Optical Coherence Tomography (Marcel Dekker Inc., New York), 2002.
4) Bonhoeffer T, Grinvald A : Optical imaging based on intrinsic signals: The methodology. In: Toga AW Mazziotta JC, eds. Brain mapping-The methods. 55-97, San Diego. Academic press, 1996.
5) Tanifuji M : The functional organization of monkey inferotemporal cortex. In: Kaas JH and Collins CE, eds. The primate visual system. 345-363, New York: CRC press, 2004.
6) Uma Maheswari R, et al : Functional optical coherence tomography to reveal functional architecture of cat visual cortex in vivo, Proc. SPIE **5140** : 77-83, 2003.
7) Uma Maheswari R, et al : Novel functional imaging technique from brain surface with optical coherence tomography enabling visualization of depth resolved functional structure in vivo. J Neurosci Methods **124** : 83-92, 2003.
8) Hubel DH : Eye, Brain and Vision. New York: Scientific American Library, 1995.

taprald4/z7g-iovs/z7g-iovs/z7g00507/z7g8167d07a | moyerr | S=11 | 3/6/07 | 19:07 | Art: 06-1294 | Input-mr

# Intrinsic Signal Imaging in Macaque Retina Reveals Different Types of Flash-Induced Light Reflectance Changes of Different Origins

AQ: 1

*Gen Hanazono,*[1,2] *Kazushige Tsunoda,*[1,2] *Kei Shinoda,*[1] *Kazuo Tsubota,*[3] *Yozo Miyake,*[1] *and Manabu Tanifuji*[2]

AQ: 2

**Purpose.** Intrinsic signal imaging is a newly developed technique that can map the light reflectance changes of tissues noninvasively. It has been used to map the functional organization of the retina by recording light-induced changes in the cone and rod photoreceptors. The purpose of this study was to investigate the properties of the intrinsic signals in the monkey's retina. To accomplish this, the intrinsic signals and the electroretinograms (ERGs) evoked by the same stimuli were measured under different recording conditions.

**Methods.** The fundus of macaque monkeys was observed with infrared light and recorded with a charge-coupled device (CCD) camera. The intrinsic signals were measured as retinal light reflectance changes induced by diffuse or focal flash stimuli. ERGs were recorded under the same stimulating conditions. The reflectance changes induced by different flash intensities, flash intervals, and background luminance were compared.

**Results.** The intrinsic signals were categorized into different groups based on the location in the fundus. Fast signals (peak: ~100 ms) were recorded from the posterior retina including the fovea, and slow signals (peak: 5.0–6.0 seconds) were recorded from the optic disc and nonfoveal posterior retina. The threshold of the slow signal changes was comparable to that of the ERG b-wave, and the thresholds of the fast signals were higher than that of the ERG a- and b-waves.

**Conclusions.** The retinal intrinsic signals are composed of several components with different response properties and different sources. This recording technique may be useful for mapping the retinal function in eyes with various disorders. (*Invest Ophthalmol Vis Sci.* 2007;48:000–000) DOI:10.1167/iovs.06-1294

Assessing the functional properties of the retina objectively is essential for making a correct diagnosis and prognosis in various retinal disorders. Although recent advances in imaging techniques—for example, optical coherence tomography (OCT),[1,2] have revealed the morphologic changes in retinal structures, the functional properties of the retina cannot be evaluated with these imaging techniques. Thus, the electroretinogram (ERG) is still the only practical method of assessing neural activities in the retina.

Intrinsic signal imaging is a well-established imaging technique that translates neural activity into a visual image. This method measures the stimulus-induced light reflectance changes in tissues and has recently been used to assess the cone- and rod-induced retinal responsiveness in macaque monkeys.[3] It has also been used to examine the near-infrared reflectance changes in the human retina[4–6] and optic nerve head.[7] This noninvasive objective technique has good potential for development as a tool for the early detection of retinal dysfunction in cases of age-related macular degeneration, retinitis pigmentosa, and other retinal diseases.

However, before this tool can be brought into the clinic, a detailed knowledge of the properties and origin of the signals obtained by intrinsic signal imaging is necessary. Based on past investigations of intrinsic signal imaging in the cerebral cortex, the decrease in light reflectance (i.e., darkening after a visual stimulus) correlates strongly with local neural activity.[8–11] In the retina, however, the source and the properties of the intrinsic signals appeared to be more complex than in the cerebral cortex due to its complex layered structure.[3]

The purpose of this study was to investigate the basic properties of the retinal intrinsic signals. To accomplish this, we recorded the intrinsic signals of the macaque retina and ERGs under various recording conditions but using the same diffuse flash stimulus. In addition, we recorded the intrinsic signals evoked by focal flash stimuli. The results indicate that the intrinsic signal of the monkey's retina is composed of different components that originate in different layers of the retina.

## Methods

The procedures used to record the intrinsic signals have been described in detail.[3]

The experiments were performed on two Rhesus monkeys (*Macaca mulatta*) and one Japanese monkey (*Macaca fuscata*). The results from monkeys 1 and 2 are shown in Figures 1 trough 5, and those from monkey 3 in Figures 6 and 7. After an intramuscular injection of atropine sulfate (0.08 mg/kg), the monkeys were anesthetized with droperidol (0.25 mg/kg) and ketamine (5.0 mg/kg) and then paralyzed with vecuronium bromide (0.1–0.2 mg/kg per hour). They were artificially ventilated with a mixture of 70% $N_2O$, 30% $O_2$, and 1.0% to 1.5% of isoflurane. The EEGs, ECGs, expired $CO_2$, and rectal temperature were monitored continuously throughout the experiments. Before the recordings, the pupils were fully dilated with topical tropicamide (0.5%) and phenylephrine hydrochloride (0.5%). The experimental protocol was approved by the Experimental Animal Committee of the Riken Institute, and all experimental procedures were performed in accordance with the guidelines of the Riken Institute and the ARVO Statement for the Use of Animals in Ophthalmic and Vision Research.

From the [1]Laboratory of Visual Physiology, National Institute of Sensory Organs, Tokyo, Japan; the [2]Laboratory for Integrative Neural Systems, Brain Science Institute, RIKEN, Saitama, Japan; and the [3]Department of Ophthalmology, Keio University School of Medicine, Tokyo, Japan.

Supported by Researches on Sensory and Communicative Disorders from the Ministry of Health, Labor, and Welfare, Japan.

Submitted for publication October 27, 2006; revised December 28, 2006; accepted Month, Day, 2007.

Disclosure: **G. Hanazono**, None; **K. Tsunoda**, None; **K. Shinoda**, None; **K. Tsubota**, None; **Y. Miyake**, None; **M. Tanifuji**, None

The publication costs of this article were defrayed in part by page charge payment. This article must therefore be marked "*advertisement*" in accordance with 18 U.S.C. §1734 solely to indicate this fact.

Corresponding author: Kazushige Tsunoda, Laboratory of Visual Physiology, National Institute of Sensory Organs, Tokyo Japan, 2-5-1 Higashigaoka, Meguroku, Tokyo 152-8902, Japan.
tsunodakazushige@kankakuki.go.jp.





ARTICLE TYPE: VNEU

tapraid4/z7g-iovs/z7g-iovs/z7g00507/z7g8167d07a | moyerr | S=11 | 3/6/07 | 19:07 | Art: 06-1294 | Input-mr



## Intrinsic Signal Imaging and Data Analyses

A modified digital fundus camera system (NM-1000; Nidek, Aichi, Japan) was used to observe and measure the light reflectance changes from the ocular fundus. The fundus images were recorded with a charge-coupled device (CCD) camera (PX-50BC; Primetech Engineering, Tokyo, Japan), and the images were digitized with an IBM-compatible computer equipped with a video framegrabber board (gray-level resolution, 10 bits; spatial resolution, 640 × 480; temporal resolution, one-thirtieth of a second; Corona II; Matrox, Quebec, Canada). The camera was focused on the macular vessels, and the area recorded covered 45°, which included the macula; the superior and inferior vascular arcades, and the optic disc. We mainly investigated three retinal sites: the fovea, the posterior retina between the macula and inferior temporal artery, and the optic disc (Fig. 1A).

F1

The fundus was continuously monitored with light from a halogen lamp filtered through an infrared interference filter (840–900 nm). Visible light could not be used for fundus monitoring because the light reflectance changes induced by bleaching of the photopigments have a polarity opposite to that of the intrinsic signals,[3,12–16] leading to incorrect mapping of the stimulus-evoked responses topographically.

Each recording trial consisted of 300 video frames collected at 30 frames per second for a total recording time of 10 seconds. To determine the time course of the flash-induced reflectance changes, we averaged the gray-scale values of 15 video frames collected in 0.5 second for each of the data points (Figs. 1, 6, and 7).

An unfiltered Xenon flash (duration: 1 ms) was given to the whole posterior pole of the ocular fundus or to a focal region of the posterior retina, 500 ms after the initiation of data acquisition. The maximum flash intensity (0-log-unit intensity) measured at the cornea was 308.0 cd · s/m$^2$ (measured at 50.2 mm from the object lens, by a photoradiometer; model IL-1700; International Light Technologies Inc., Peabody, MA). The timing of the data acquisition and stimulus delivery was under computer control.

Changes in light reflectance from the ocular fundus after the stimulus, such as a darkening (a decrease in light reflectance), and a brightening (an increase in light reflectance), of the retina, were measured. Under infrared observation, the light reflectance of the whole posterior retina decreased (the fundus image became darker) after a flash stimulus (Fig. 1B). The optical signal was calculated as follows: (1) the gray-scale values of the image obtained after the

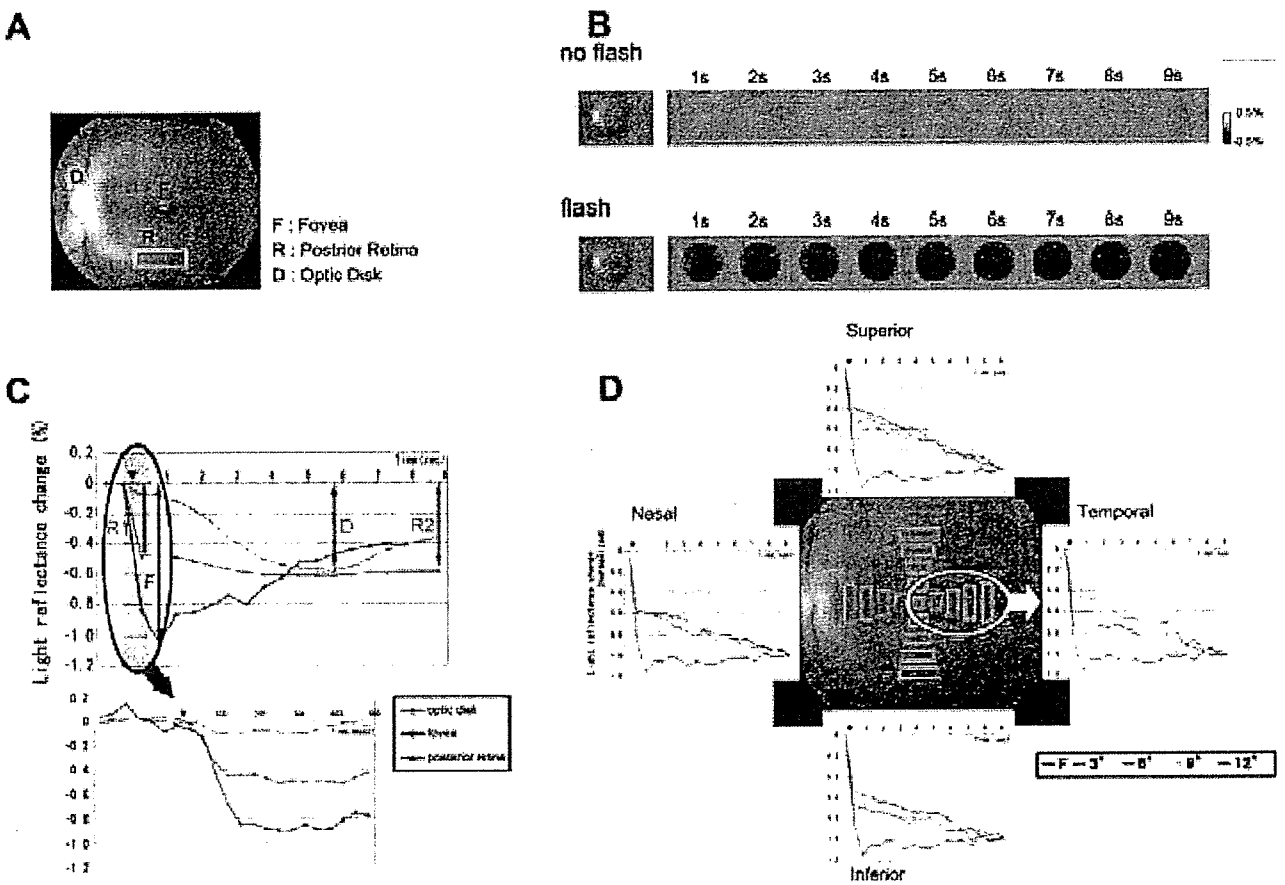


COLOR

FIGURE 1. Fundus photograph and time courses of intrinsic signals after a flash stimulus. (**A**) Fundus photograph of normal retina showing the regions analyzed. (**B**) Time courses of two-dimensional images of ocular fundus showing the light reflectance changes during a 10-second trial without (*top*) and with (*bottom*) a flash stimulus. *Left*: fundus images taken at the beginning of a trial; *right*: light reflectance changes after a flash. Thirty consecutive video frames collected during 1 second were averaged for one poststimulus fundus image. Darkened regions indicate a decrease of light reflectance after the flash stimulus. (**C**) Plot of the time courses of light reflectance changes in a single trial after a diffuse flash stimulus in the three locations shown in (**A**). The time after the flash is shown on the abscissa. *Arrowhead*: point of delivery of the flash. Each point is the average of 15 video frames collected during 0.5 second of the light reflectance changes. *Colored arrows*: **F** signal at fovea, **D** signal at the optic disc and **R1** and **R2** signals in the nonfoveal posterior retina. The time course of the reflectance changes during the first 500 ms after a flash is shown in the *bottom* graph where each point is the average of two video frames during one-fifteenth of a second. (**D**) Time courses of light reflectance changes in a single trial after a diffuse flash, measured at the fovea and four different regions within 12° from the fovea in each quadrant. Amplitudes are indicated as values relative to the light reflectance changes at the end of each trial (1.0). The four regions tested in each quadrant are indicated as distances from fovea (3°, 6°, 9°, and 12°).

taprakd4/z7g-iovs/z7g-iovs/z7g00507/z7g8167d07a | moyerr | S=11 | 3/6/07 | 19:07 | Art: 06-1294 | Input-mr



stimulus were divided, pixel by pixel, by those obtained during a 0.5-second period before the stimulus, and (2) this ratio was rescaled to 256 levels of gray-scale resolution to show the stimulus-induced reflectance changes.

A deterioration of the signal can be caused by movement artifacts: small involuntary eye movements, blood pressure pulsations, and respiration-associated movements. Eye movements are the most serious artifacts because a different fundus position would be analyzed during the pre- and poststimulus periods. However, these artifacts can be minimized by giving sufficient amounts of muscle relaxants to block eye movements. Pulsations cause small movements of the retinal arteries and optic disc. However, the pulsation-derived reflectance changes are less than one tenth of the stimulus-induced reflectance changes and are almost negligible if 15 video frames are averaged during the 0.5 seconds (Fig. 1G).

Artifacts from respiratory movements produced large light reflectance changes, which were 20% to 40% of the stimulus-induced reflectance changes. This artifact is due to changes in blood flow or volume and periodic back-and-forth movement of the eye, synchronized with the respiration. In our recordings, the respiration-induced artifacts were significant, and the respirator had to be stopped during a recording period of 10 seconds. With the respirator stopped, we could record stable intrinsic signals whose quality was sufficient to map the retinal reflective changes in a single trial without either averaging or offline analysis with realignment of the images.[6]

To measure the time course of the signal changes, we recorded two trials under the same conditions and averaged the results. We found that each trial had to be recorded with at least a 20-minute interval to allow a recovery of the signal production from the previous stimulus. Thus, in experiments where the 11 stimulus intensities were recorded, up to 7 to 8 hours were necessary to record two trials under each condition. Because only two recordings were obtained under each recording condition, the type of statistics that could be used was limited. Unlike ERG recordings, the amplitudes of intrinsic signals are vulnerable to changes in the heart rate, blood pressure, and corneal reflectance. Because it is critical for quantitative comparisons to measure the responses under the same physiological conditions, averaging many trials was impractical for our experimental protocol.

## Electroretinograms

A bipolar contact lens electrode (Mayo, Aichi, Japan) was used to record the ERGs. The ERGs were amplified ×10,000 and the band-pass filters were set at 0.3 to 500 Hz (Power Lab; AD Instruments, Colorado Springs, CO). A 15- brief white xenon flash stimulus was delivered through the same observation optical system to stimulate the retina while the fundus was monitored with the infrared observation light. As in intrinsic signal imaging, two ERGs were recorded for each recording condition and were averaged.

## Recording Conditions

Initially, we compared the responses of the intrinsic signal images and the ERGs evoked by the same diffuse flash stimulus under different recording conditions: (1) flash intensities (Supplementary Fig. S1; all supplementary figures are online at [INSERT URL]), (2) flash intervals (Supplementary Fig. S2), and (3) background luminance (Supplementary Fig. S3). Second, we stimulated the retina focally and measured the intrinsic signals in the stimulated and nonstimulated regions.

**Flash Intensity.** The maximum intensity of the xenon flash was 308.0 cd · s/m$^2$, and neutral density filters were used to attenuate the intensity. The intrinsic signals and ERGs were recorded over an 8.8-log-unit range in 11 steps (−8.8, −7.8, −6.7, −6.0, −4.8, −3.7, −3.0, −1.8, −0.7, −0.3, and 0.0). The recordings were performed consecutively with 20 minutes between changes in the intensity under both the dark- and light-adapted conditions. In the light-adapted condition, each recording was followed by 10 minutes of light adaptation. For light adaptation, an 80-mm diameter white polyethylene ball, similar to a ping-pong ball, was cut in half and placed between the fundus camera and the eye. The ball was illuminated by two halogen lamps through fiber optics so that the luminance in the center was 30 cd/m$^2$. Although the luminance of the ball was not spatially uniform, we believe, that this did not affect the results of the experiments significantly because the luminance at 10° from the center varied by only 94.4% to 103.0% relative to the center (100%). The illuminated ball was removed a few seconds before each recording trial.

**Flash Intervals.** The intrinsic signals and ERGs were recorded after 0.5, 1.0, 3.0, 5.0, 10, 30, and 60 minutes of flash-to-flash intervals. After a 30-minute recovery period, the posterior retina was first bleached by a strong white flash stimulus (bleaching flash: −0.3 log units; 1.5-i × 10$^2$ cd · s/m$^2$), followed by the various interval times listed. The intrinsic signals and ERGs were then measured with a flash (recording flash) of the same intensity as the bleaching flash.

**Background Luminance.** The background luminance was changed from 0 to 200 cd/m$^2$ in five steps, to examine the effects of background luminance on the intrinsic signal images. For the intrinsic signal imaging, a strong white flash (−0.3 log units; 1.5-i × 10$^2$ cd · s/m$^2$) was used as a stimulus. For the ERGs, the flash intensity, that evoked the maximum b-wave (−3.0 log; 3.08 × 10$^{-1}$ cd · s/m$^2$) was used.[17] Each recording trial was recorded with a 20-minute interval.

Finally, a focal stimulus was projected onto the retina by inserting a transparent film in the optical pathway of the Xenon strobe. The film was placed at a point that was conjugate to the retina. The shape and size of the stimulus on the retina was determined by the pattern on the film.

# Results

The time course of the intrinsic signals evoked by a brief flash stimulus was different for different regions of the ocular fundus. A representative flash-evoked response from a single trial under dark-adapted condition is shown in Figure 1C. The reflectance changes at the fovea were rapid and reached a negative peak (darkening) within 100 to 200 ms after the flash. The darkening then gradually returned to the prestimulus baseline. The changes in the signals at the optic disc were much slower and reached a peak 5 to 6 seconds after the flash. The signals in the nonfoveal posterior retina were composed of both fast and slow components. The light reflectance decreased rapidly within 100 ms (flexural point) and then gradually decreased, reaching a trough 5 to 6 seconds after the flash. As shown in Figure 1D, the time course of the intrinsic signals of the posterior retina was approximately the same over the whole field except for the small central region within the avascular foveal area (i.e., 300 μm in diameter).[18] The light reflectance at the fovea did not decrease after the initial negative peak.

There is some evidence that the signal in the nonfoveal posterior retina is composed of at least two components. First, the threshold of the fast and slow signals were different by 1 log units of flash intensity in the dark-adapted condition and 1 or 2 log units in the light-adapted condition, as shown by the following results. Only the later phase of the slow reflectance change was observed after a dim flash stimulus. Second, only the amplitude of the late phase of the signal is vulnerable to changes in the heart rate, whereas that of the early phase is not changed (see the Discussion section).

To analyze the flash-induced intrinsic signals and electrophysiological responses, we used the value of the initial peak of light reflectance change at the fovea (E: 15 × 15 pixels), the value at the flexural point of light reflectance change (R1), or the value at the end of the recording trial (R2) in the inferior retina (60 × 40 pixels), and the lowest value of light reflectance at the optic disc (D: −70 × 50 pixels; Fig. 1C). AQ: 3

## Stimulus Intensity

The intrinsic signal images and ERGs recorded after a diffuse flash are shown in Figures 2A, 3A, 4A, and 5A, and the intensities of the intrinsic signals and ERG amplitudes are shown in Figures 2B, 3B, 4B, and 5B.

F2 Under dark-adapted conditions (Fig. 2), the amplitudes of a- and b-waves of the ERGs increased as the stimulus intensity increased.[19] The intrinsic signals of **D** and **R2** had the same threshold as that of the b-wave, and their amplitudes also increased as the intensity increased. The amplitudes of **D** and **R2** reached a plateau at −6.0 log units and did not change significantly with higher intensities. **R2** increased again with higher flash intensities over −0.3 log unit in monkey (M)1 and −0.7 log unit in M2.

The threshold of **R1** was higher than that of **D**, **R2**, and the ERG a-wave. The amplitude of **R1** increased gradually with increasing flash intensities. The amplitude of **F** also increased with increasing flash intensities, but its threshold was higher than that of any of the other intrinsic signals.

Under light-adapted conditions (30 cd/m$^2$), the amplitudes of the a- and b-waves increased progressively with increasing flash intensities, but that of the b-wave decreased with intensities higher than −3.0 log units, due to the photopic hill

F3 phenomenon (Fig. 3).[17] The thresholds of **D** and **R2** of the intrinsic signal images were higher than those in the dark-adapted condition by 2.1 log units in M1 and 2.8 log units in M2. The thresholds of the **D** and **R2** signals and ERG a- and b-waves were the same in M1.

The threshold of **R1** was the same in both dark- and light-adapted conditions. In both conditions, the threshold of **F** was the same in M1 but was 0.7 log unit lower than that in M2 in the dark-adapted condition. What was striking was that the amplitude of **R2** was smaller with brighter flashes in M2 under light-adapted conditions and the light reflectance change became approximately zero at −0.3-log-unit intensity. There was a tendency for the amplitude of the **R2** signal to decrease with intensities that were 1.0 to 2.0 log units higher than the threshold of the **R1** signal.

## Effect of Changes in Flash Intervals

After a bleaching with a bright flash, the amplitudes of the a- and b-waves were reduced and the amplitudes increased with increasing time in the dark (Fig. 4).[20,21] The recovery of the F4 ERG amplitudes appeared slower than that in other studies because our flash intensity was 1.7 log units more intense than that of the ISCEV (International Society for Clinical Electrophysiology of Vision) standard flash.

For the intrinsic signals, only the **F** signal had a pattern similar to that of the ERGs (i.e., the amplitude increased gradually with longer intervals in the dark after the preceding flash). **D**, **R1**, and **R2** had peaks at 3 to 5 minutes after the preceding flash, and the amplitudes decreased at 10-minute intervals. These findings indicate that the source of the intrinsic signals of the optic disc and the nonfoveal posterior retina are different from that of the fovea.

## Effect of Background Luminance

The amplitudes of the a- and b-waves decreased progressively as the background illumination increased (Fig. 5).[22,23] The F5 amplitudes of **D** and **R1** of the intrinsic signals under light-adapted conditions (10–200 cd/m$^2$) were 45% to 65% as large as that in the dark-adapted condition in M1 and 60% to 80% in M2. The amplitude of **F** in the light-adapted condition was approximately 90% as large as that in dark-adapted condition in M1 and 80% to 100% in M2.

In contrast, the **R2** signal, was markedly decreased under light-adapted conditions. Even with a weak background of 10 cd/m$^2$, **R2** was decreased by approximately 90% in M2, and an increase of 20% in light reflectance was observed in M1. This

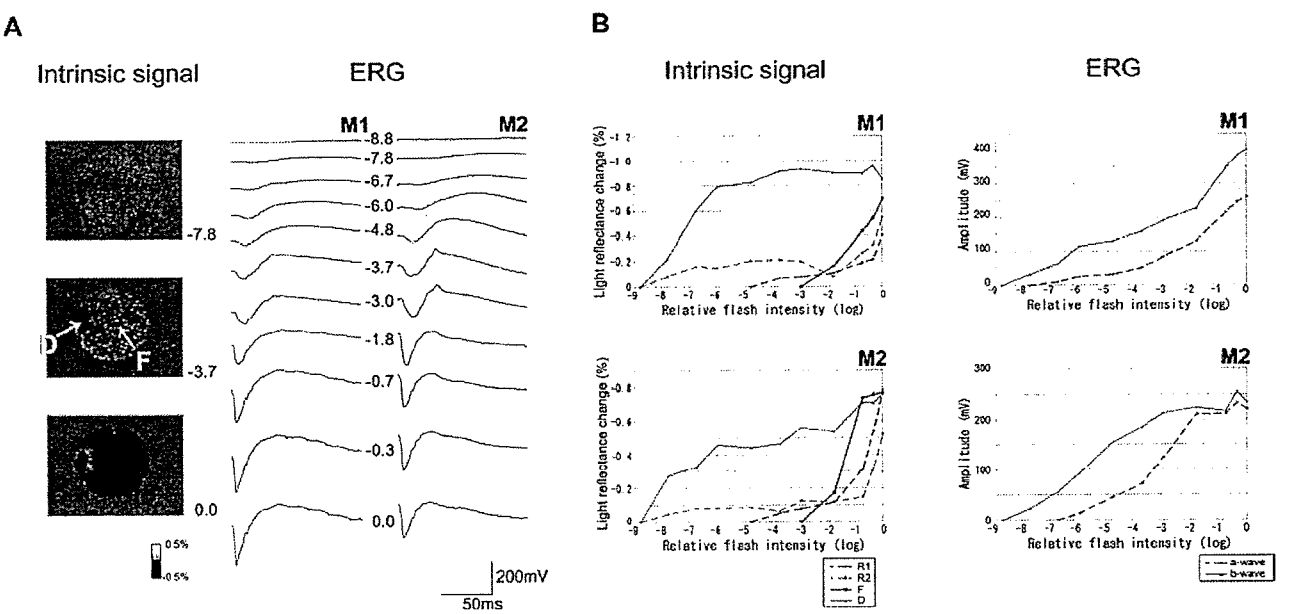


FIGURE 2. Intrinsic signal images and ERGs after a diffuse stimulus in dark-adapted conditions. (**A**) Fundus images of the intrinsic signals (*left*) and ERGs (*right*) after a diffuse flash in the dark-adapted condition with stimulus intensities from −8.8 to 0 log units. *Left*: intrinsic signal images from a single trial averaged from 5.0 to 8.0 seconds after the flash. The darkened region in fundus images indicates light reflectance decrease after the flash. The ERGs recorded from monkeys M1 and M2 are shown. The relative log flash intensity responses to the maximum flash are indicated. D: optic disc, F: fovea. (**B**) *Left*: amplitudes of **R1**, **R2**, **F**, and **D** of the intrinsic signals in response to increasing flash intensities are shown as light reflectance changes for M1 and M2. *Right*: the amplitudes of the ERG a- and b-waves in response to the same stimulus series. Note that negative values of light reflectance changes are plotted to indicate the strength of intrinsic signals.

tapraid4/z7g-iovs/z7g-iovs/z7g00507/z7g8167d07a | moyerr | S=11 | 3/6/07 | 19:07 | Art: 06-1294 | Input-mr



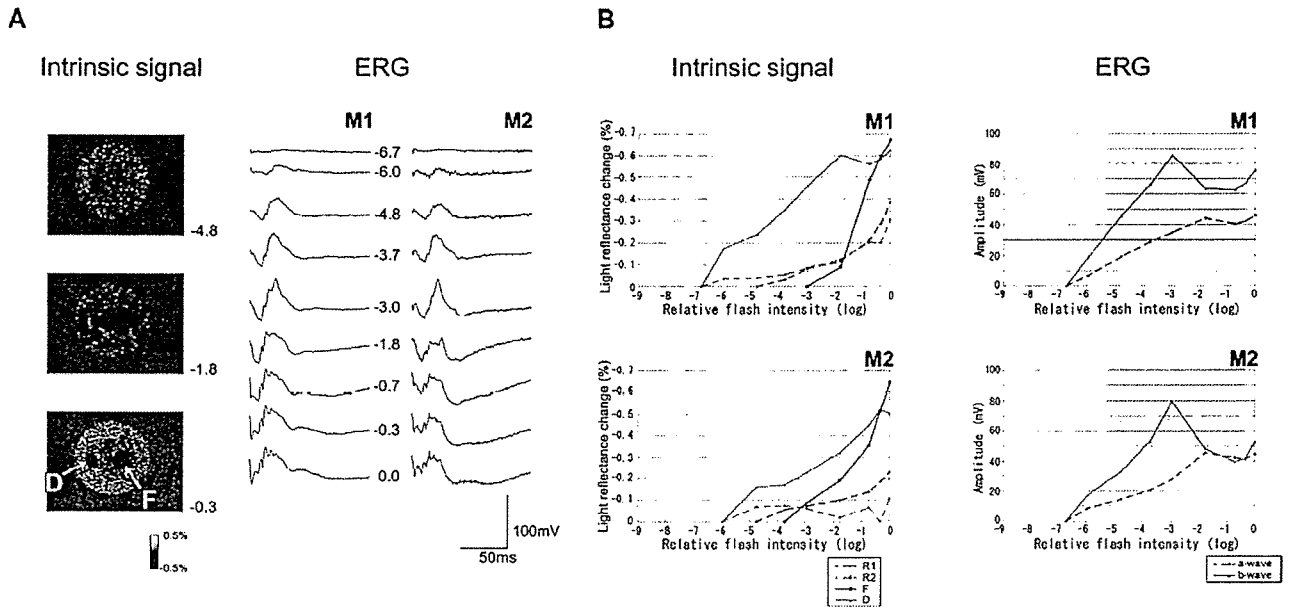


FIGURE 3. Intrinsic signals and ERGs after a diffuse stimulation under light-adapted conditions. (A) Fundus images of the intrinsic signals (*left*) and ERGs (*right*) after different stimulus intensities (−6.7–0 log-unit intensity). Representative signal images for a single trial averaged from 5.0 to 8.0 seconds after a flash are shown. (B) Amplitudes of R1, R2, F, and D of the intrinsic signals and the a- and b-waves of the ERGs in response to various flash intensities are as described in Figure 2.

means that the posterior retina appeared brighter after a flash at the later phase of a recording trial with bright background illumination.

## Responses at Optic Disc

We have shown that the thresholds of the light reflectance changes at the optic disc were comparable to the threshold of the ERG b-waves and that even a dim stimulus can evoke a strong signal at the optic disc (Fig. 2). To determine the contribution of blood-related changes to the intrinsic signals at the optic disc, we measured the responses from different regions within the optic disc (Fig. 6A): (1) the central region where the central retinal artery and vein run perpendicular to the imaging plane (Center), (2) over the superior branch of the central retinal artery (Artery), (3) over the superior branch of the central retinal vein (Vein), (4) temporal and nasal regions

F6

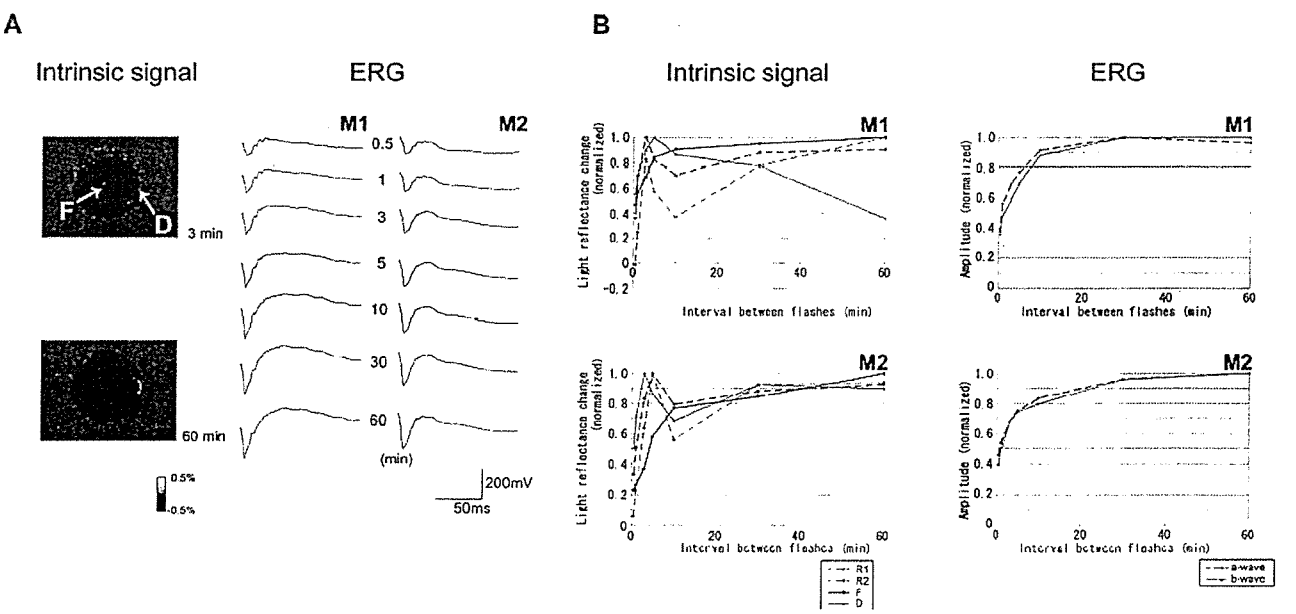


FIGURE 4. Intrinsic signals and ERGs after a diffuse stimulus recorded at different times after bleaching. (A) Fundus images of intrinsic signals (*left*) and ERGs (*right*) evoked by a diffuse flash (−0.3 log unit) at different intervals (0.5–60 minutes) after a bleaching flash at the same intensity. Representative images from a single trial averaged from 5.0 to 8.0 seconds after a flash are shown. (B) Amplitudes of R1, R2, F, and D of the intrinsic signals and a- and b-waves of the ERGs at different flash intervals. Amplitudes are relative to the maximum for each signal component.

taprate4/z7g-iovs/z7g-iovs/z7g00507/z7g8167d07a | moyerr | S=11 | 3/6/07 | 19:07 | Art: 06-1294 | Input-mr



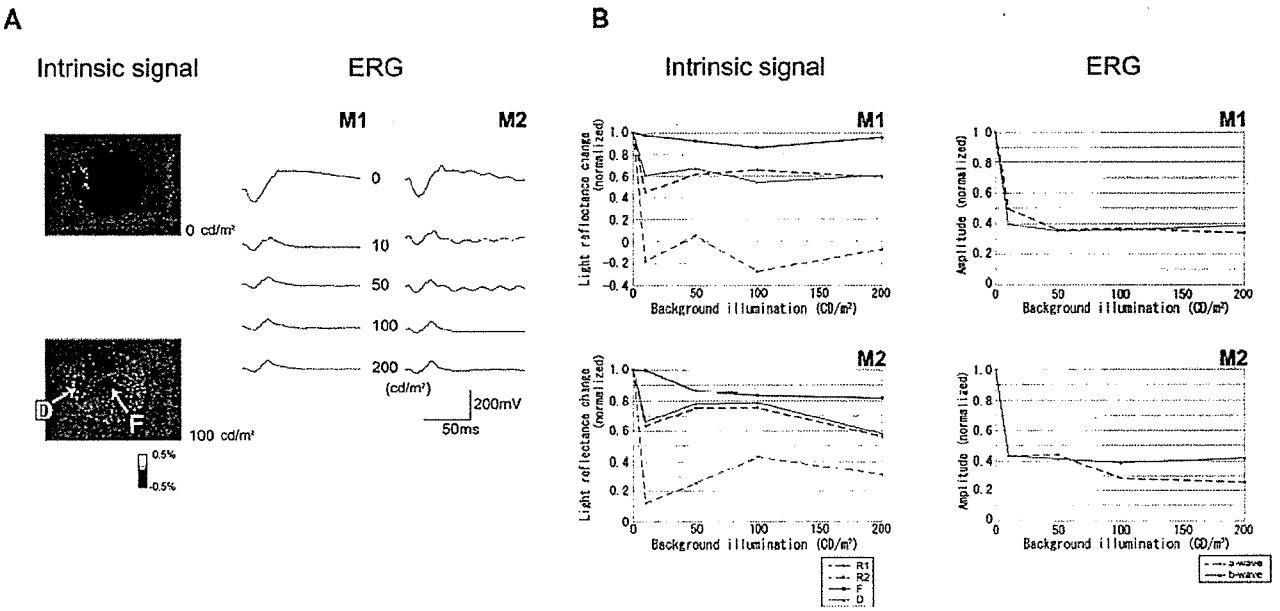


FIGURE 5. Intrinsic signal images and ERGs after a diffuse flash stimulus on different background luminances. (A) Fundus image of intrinsic signals (*left*) and ERGs (*right*) after a diffuse flash on different background luminances (0–200 cd/m$^2$). Representative signal images in a single trial averaged from 5.0 to 8.0 seconds after a flash (−0.3 log unit) are shown. For the ERGs, a flash with the maximum intensity which evoked a b-wave without photopic hill phenomenon was used (−3.0 log units). (B) Amplitudes of R1, R2, F, and D of the intrinsic signals and the ERG a- and b-waves with different background luminances. Amplitudes are relative to the maximum for each signal component.

where large vessels are not present (Temporal and Nasal), and (5) the entire optic disc (D). A diffuse flash of −0.7 log unit intensity was used for stimulation, and 17 consecutive trials with 3-minute intervals were averaged.

The light reflectance changes were especially large in the central region where the central retinal artery and vein pass through the optic nerve (three times larger than that in the whole region; Fig. 6B). The light reflectance changes over the superior branch of the central retinal artery and vein were 1.2 times larger than that of the whole region. Although the size of the intrinsic signals varied in different regions within the margins of the optic disc, the time course at each region seemed to be almost the same (Fig. 6C).

## Focal Stimulation

The recording of the focal macular ERG is a technique used to measure the electrical responses in the macula by focally stimulating the macular region.[24,25] Focal flash stimuli can be given to the posterior retina with our recording system, however, our system is not setup to deliver a background illumination to suppress the rod responses and cannot measure the electrical activity in the stimulated region. We have stimulated focal regions of the posterior retina, and compared the time course of the intrinsic signals in both the stimulated and nonstimulated regions in dark-adapted conditions.

First, the macular area including the fovea was focally stimulated with an 8.8° circular stimulus (Figs. 7A, 7B). The light F7

COLOR

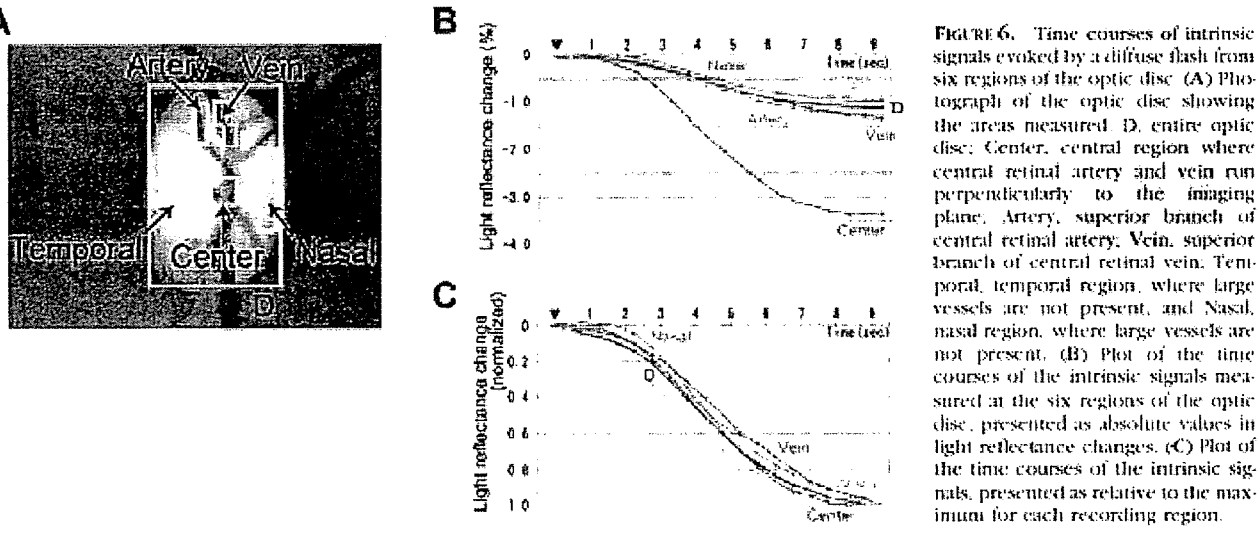


FIGURE 6. Time courses of intrinsic signals evoked by a diffuse flash from six regions of the optic disc. (A) Photograph of the optic disc showing the areas measured. D, entire optic disc; Center, central region where central retinal artery and vein run perpendicularly to the imaging plane; Artery, superior branch of central retinal artery; Vein, superior branch of central retinal vein; Temporal, temporal region, where large vessels are not present; and Nasal, nasal region, where large vessels are not present. (B) Plot of the time courses of the intrinsic signals measured at the six regions of the optic disc, presented as absolute values in light reflectance changes. (C) Plot of the time courses of the intrinsic signals, presented as relative to the maximum for each recording region.

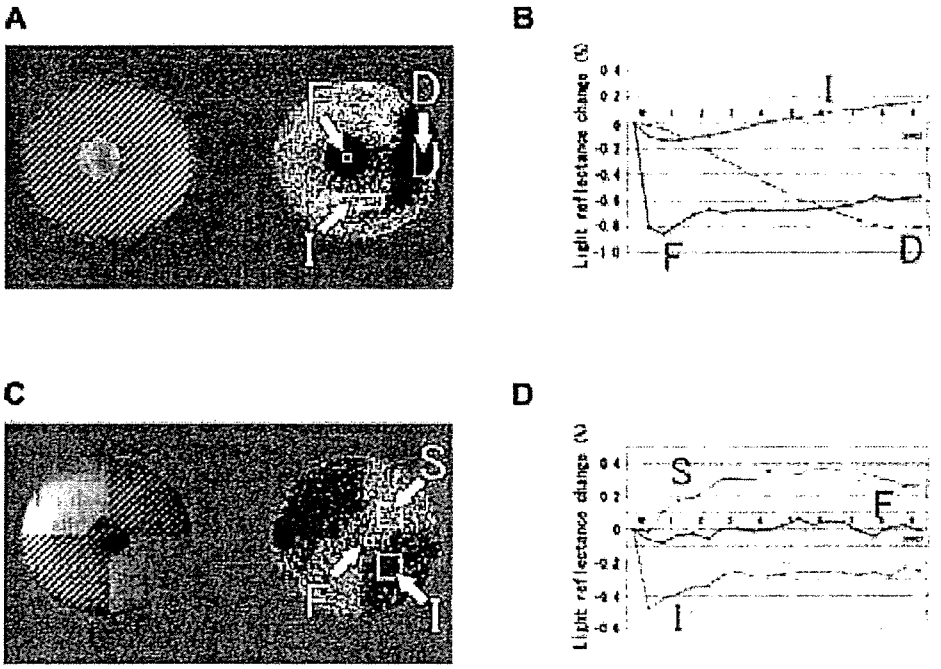


FIGURE 7. Effect of focal stimulus on the intrinsic signals. (A) *Left*: fundus image showing circular focal stimulus in the macula including the fovea (8.8° in diameter). The stimulus was blocked over the *hatched area*. Regions for time course analysis are indicated as F (fovea), D (optic disc), I (inferior retina within the vascular arcade, sparing thick vessels). *Right*: fundus image of intrinsic signal evoked by the focal stimulus, averaged from 6.5 to 9.5 seconds after stimulation. Data from four consecutive trials were averaged. (B) Plot of the time courses of light reflectance changes in a single trial after a focal flash at the three locations shown in (A). (C) *Left*: fundus image showing mosaic-like focal stimulus in the posterior pole, sparing central 8.0° including fovea. Regions for time course analysis are indicated as F (nonstimulated fovea), S (stimulated superior retina), and I (nonstimulated inferior retina). Right: two-dimensional image of intrinsic signal evoked by the focal stimulus, averaged from 6.5 to 9.5 seconds after stimulation (single trial). (D) Plot of the time courses of light reflectance changes in a single trial after a focal flash at the three locations shown in (C).

COLOR

reflectance in the stimulated region decreased (Fig. 7B; F) and the region that darkened exactly matched the location of the stimulus (Fig. 7A). In contrast, the region without stimulation became brighter at the later phase of a recording trial (Fig. 7B; I). When two quadrants of the posterior retina were stimulated with the macula spared, the intrinsic signal showed exactly the same darkening pattern as the shape of the stimulus (Fig. 7C). The stimulated posterior retina (I) showed a negative R1 and negative R2 signal (i.e., a darkening; Fig. 7D). The nonstimulated area of the posterior pole (S) was brighter (positive R2), which is usually not observed under other recording conditions. The fovea (F), where the stimulus was masked, did not show any light reflectance changes after the flash.

## DISCUSSION

The origin of the intrinsic signals in the cerebral cortices has been extensively investigated; however, most of the studies have dealt with the deoxygenation of hemoglobin.[8,9,11] The standard hypothesis is that the intrinsic signals in the cerebral cortex arise from light reflectance changes due to the many metabolic changes after neural activation. For example, the intrinsic signal measured at 570 nm is dominated by changes in the blood volume in the capillaries; that at 600 to 650 nm is dominated by the changes in the deoxygenation level of hemoglobin, and that in the infrared region is dominated by changes in tissue light scattering. Although different metabolic changes are highlighted at different wavelengths, the optical responses obtained at these wavelengths had nearly the same spatial pattern of activation as that of the activated neurons.[9,26] Whatever wavelength was chosen for the measurement of reflectance, the most critical premise for evaluating the intrinsic signal has been that it is the darkening (i.e., a decrease in light reflectance), that correlates with the local neural activity. This is more or less true of the intrinsic signal images in the retina[3]; however, the spatial distribution of the signals appeared to be more complicated when the retina is focally stimulated.

Our goal was to find out what each signal component represented by comparing the intrinsic signals with the ERGs recorded under the same conditions. Although the spatially localized responses of the intrinsic signals cannot be directly compared with the responses in full-field ERGs, this comparison may provide us with some keys to determine the possible mechanisms of the production of the intrinsic signals, because the neuronal mechanisms of the production of the ERGs have been well investigated.

It is important to understand that, in principle, the intrinsic signals are not necessarily produced by photoreceptors. There may be differences in the site of the photoreceptor and the site for producing the signals. The light reflectance changes reflect the summation of the stimulus-evoked metabolic changes happening in the 10 retinal layers, each of which may produce signals with different characteristics. The same difficulty arises when the origin of the different components of the ERGs is investigated. Thus, the type of activated photoreceptors and

the location where the signal is produced should be carefully separated.

## D Signals

The threshold of the **D** signal was comparable to that of the ERG b-wave in the dark-adapted condition (Fig. 2).[19] The threshold was higher by 2.0 to 3.0 log units under light-adapted conditions (Fig. 3),[17] and the amplitude was greatly decreased in the presence of background illumination (Fig. 5).[22,23] These results indicate that the **D** signal evoked by a dim flash (weaker than −5.0 or −6.0 log units) under dark-adapted conditions reflects the activation of rod photoreceptors, and those evoked by stronger flash reflects the activation of both cone and rod photoreceptors. The **D** signal evoked under light-adapted conditions reflects mainly the activation of the cone photoreceptors.

The time course of the **D** signal is slow and is probably produced by a flash-induced blood volume or flow increase. The decrease in light reflectance is due to the increased light scattering of the red blood cells. Previous studies have shown that flashing lights can increase the blood flow at the optic disc of humans and cats.[27,28] An increase in blood volume is known to decrease the reflectivity of tissues due to the increased scattering of light by the red blood cells in the blood vessels.[11,29] Although a change in the blood volume or flow was not directly measured in this study, the results of measurements of the intrinsic signals on the optic disc support this (Fig 6). In the central region of the optic disc occupied by the central retinal artery and vein, the reflectance changes were three times greater than in other regions, although the time course was almost the same as at any locations within the optic disc. The light-scattering changes induced by changes in the blood volume or flow may be most effectively observed when the vessels are perpendicular to the imaging plane. Even in the white regions (Fig. 6A, Temporal and Nasal), where large vessels are not present, the light reflectance changes showed a time course similar to that in the central region (Fig. 6C) indicating that this signal is derived from the blood volume or flow changes in the capillaries. As for the question of whether the blood volume or flow contributes more significantly to this signal, we do not have any evidence to conclude which has the greater role and recommend that the mechanism of blood-related light scattering changes be thoroughly investigated.

Neural activity in the optic nerve causes shrinkage of the extracellular space due to cellular swelling, and this was detected optically by intrinsic signal imaging in rats.[30,31] We believe that part of the scattering changes may be due to swelling of the axons of the ganglion cells or of the glial cells. Its contribution to the whole intrinsic signal, however, may be masked by the relatively large reflectance changes due to changes in blood volume or flow. A contribution by the changes in deoxygenated hemoglobin concentration in the capillaries to the intrinsic signal may also exist, although it is believed to be negligible compared with that of tissue light scattering under infrared light observation.[9,11]

## R2 Signals

The properties of the **R2** signal were similar to those of the **D** signal, except that **R2** became very small and in some cases became positive under light-adapted conditions (Figs. 3B, 5B). The **R2** signal is probably a complex of different components and origins because the posterior retina is a complex layered structure, and its signal properties cannot be explained simply by the blood volume or flow changes in the capillaries.

We suggest that the inner retina may be the main contributor to the **D** and **R2** signals because this type of slow signal was not observed at the fovea, which lacks the inner retinal layers including the blood vessels.[18] Our data did not allow us to determine which type of cells contribute the most to the flash-evoked responses observed at the optic disc or the posterior retina.

We attempted to keep the systemic condition of the anesthetized monkeys as constant as possible during the data acquisition. In some trials, however, the heart rate became unstable and rapid changes occurred during consecutive recordings under the same stimulus conditions. For example, the heart rate increased from 120 per minute to 140 per minute during two consecutive trials in one monkey. Although such data obtained under unstable conditions were discarded, we did note that it was always the amplitudes of **D** and **R2** signals that were affected by the changes in the heart rate. In contrast, the amplitudes of **F** and **R1** signals were much less affected by changes in heart rate (data not shown). This observation suggests that the **D** and **R2** signals are related to blood-induced changes more than are the **F** and **R1** signals.

It was interesting that the amplitudes of **D** and **R2** signals were largest with 3- to 5-minute flash intervals (Fig. 4B). This finding is very different from the results of ERGs. It is possible that the mechanism by which neural activity is converted to the vascular response (i.e., neurovascular coupling)[32,33] is most effectively activated when the stimuli are given repeatedly at intermediate intervals. This possibility should be investigated more extensively.

## F Signals

The **F** signal, which is the average of light reflectance changes within the central 300 $\mu$m in diameter was faster than the **D** and **R2** signals and reaches its peak within 100 to 200 ms (Fig. 1C). The threshold for the **F** signal was much higher than any other signals and was the same in both dark- and light-adapted conditions. The characteristic anatomic structure of the fovea (viz., the absence of rod photoreceptors, capillaries and other inner retinal layers), indicates that the **F** signal reflects the activation of cone photoreceptors under any recording conditions.

The light-scattering changes due to the microstructural changes after activation of the cone photoreceptors are probably the source of the **F** signals because the foveal avascular region is free of capillaries and not subject to the changes in hemoglobin concentration or blood volume after neural activation.[18] Recent functional OCT studies using blood-free slice preparations showed that the reflectance in the photoreceptor layer is strongly changed by neural activation followed by microscopic morphologic changes.[34,35]

## R1 Signals

The amplitude of the **R1** signal increases with an increase in stimulus intensity under both dark- and light-adapted conditions as did the **F** signal. The threshold of **R1** lies between the threshold for the optic disc and fovea and was the same under both dark- and light-adapted conditions. This leads us to think that cone photoreceptors mainly contribute to the **R1** signal, because bleaching of rods in the bright condition did not change the **R1** threshold. It is difficult to assume, however, that rod and cone photoreceptors play different roles in light reflectance changes.

The property of the **R1** signal is complicated in another way. The abrupt darkening after a flash may well be explained by the photoreceptor responses like the **F** signal, but the results in Figure 4B strongly suggest that **R1** share the same signal origin with **D** and **R2** signals. The amplitude of **R1** signal did not increase with longer interstimulus intervals, but attained a maximum with 3- to 5-minute intervals as with the **D** and **R2** signals. We suggest that the **R1** signal is produced not

tapraid4/z7g-iovs/z7g-iovs/z7g00507/z7g8167d07a | moyerr | S=11 | 3/6/07 | 19:08 | Art: 06-1294 | Input-mr



TABLE 1. Properties of Four Components in Retinal Intrinsic Signals

| | Signal Components | | | |
|---|---|---|---|---|
| | D | F | R1 | R2 |
| Time to the peak in amplitude | Slow | Fast | Fast | Slow |
| Threshold in dark adaptation (log unit) (ERG a-wave, −6.7; b-wave, −7.8) | −7.8 | −1.8 | −4.8 | −7.8 |
| Threshold shift in light adaptation | ++ | − | ± | ++ |
| Increase in amplitude with shorter flash intervals (3–5 min) | + | − | + | + |
| Decrease in amplitude by light adaptation | + | ± | + | ++ |
| Possible sources | | | | |
| Contribution of blood-related light reflectance changes | ++ | − | ? | ++ |
| Contribution of inner or middle layer | ++ | − | +? | + |
| Contribution of outer layer | − | ++ | +? | +? |

only by photoreceptors but also by other inner or middle layer structures, although our data do not provide any evidence for the exact origin.

A summary of the various properties in four signal components is shown in Table 1. T1

## Focal Stimulation

Focal stimulation of the retina is one way to evaluate local neural activity in a dysfunctional retina and has been applied clinically with the focal macular ERG.[24,25] The intrinsic signals measured with focal stimuli showed that this technique can also be used to study local responses. The focally stimulated region showed a decrease in the light reflectance after the stimulus, and this darkened region exactly matched the location of the focal stimulus (Figs. 7A, 7C). It was striking that the nonstimulated posterior pole showed a slow light reflectance increase after a fast light reflectance decrease (Fig. 7B; I). In another case, the nonstimulated posterior pole showed only a light reflectance increase (Fig. 7D; S).

The brightening observed in the nonstimulated region in later phase (Fig. 7B, I; Fig. 7D; S) may be explained by (1) some type of horizontal interaction by, for example, horizontal cells, through which stimulated neurons could affect the reflectivity of the neurons outside the stimulated region, or (2) the spatial interaction in the intrinsic signals between the stimulated and nonstimulated regions via an inhomogeneous distribution of capillary blood flow.[8,9,11,56] These explanations, however, do not account for the strong and homogeneous brightening over the whole posterior region triggered by a small focal stimulus.[37] It is possible that the properties of the signals, such as polarity and threshold, are different in different retinal layers, and the difference in signal time course between stimulated and nonstimulated regions would reflect the difference of layers that mainly contribute to the light reflectance changes.

Recently, OCT imaging of neural activity has been demonstrated in the feline visual cortex,[38] isolated frog and rabbit retina,[34,35] and intact rat retina.[39] Functional OCT studies in slice preparations have revealed the complex nature of flash-evoked changes in the reflectances from various intraretinal layers: a decrease of near infrared scattering in the photoreceptor layer and an increase in the ganglion cell layer,[34] or a decrease in the photoreceptor inner segment and increase in the internal plexiform layer and photoreceptor outer segments.[35] Srinivasan et al.[39] first reported the results of functional OCT signals in the intact retina and demonstrated the flash-evoked reflectance increase in the photoreceptor outer segments. In these studies, the increase in light reflectance after a flash was mainly observed in the photoreceptor layer, whereas the decrease was mainly observed in monkey and human retinas.[5,6] This difference in signal polarity may be attributable to the difference in the methods used to measure the reflectances. In addition, other factors, such as the use of sectioned preparations that lack the RPE layer and blood supply, differences among species, and differences in the recording region in the retina, should also be considered.

The light-scattering changes after a flash observed in functional OCT is thought to be derived from the structural changes in the outer segment discs, membrane hyperpolarization, cell swelling, and changes in the composition of the interphotoreceptor matrix.[54,55] These sources can also explain the rapid light reflectance changes (F and R1) observed in our study. As suggested by our results and those of functional OCT studies of retinal sections, the characteristics of the light reflectance changes after a flash are different in different layers and different retinal locations and may be far more complex than the conventional idea of intrinsic signals mainly investigated in the cerebral cortex.[8,9,11] Interpretation of the retinal intrinsic signal is thus difficult, and maximum care should be taken in choosing the proper recording conditions and which signal is most closely correlated with the neural activities of the retina.

In conclusion, our results showed that the intrinsic signals in the retina are composed of several components of different origins, although the precise cellular mechanisms of signal production were not determined. The sensitivity of intrinsic signal images was high enough to detect weak neural activity in the retina (e.g., the slow signals in the posterior retina and the optic disc were as sensitive as the ERG b-wave in the dark-adapted condition). Moreover, the distribution of intrinsic signals reflects not only the cellular distribution in the retina but the current level of the activities. Although the source of the signal was much more complex than initially thought, by carefully selecting the proper recording condition, this imaging technique may have a potential to estimate the neural responses of different origins and obtain more useful information about various types of retinal disorders with different etiologies than the conventional electrophysiological examinations such as full-field ERGs, focal macular ERGs, and multifocal ERGs.

## *Acknowledgments*

The authors thank Uma Maheswari Rajagopalan for critical comments on the manuscript

## *References*

1. Huang D, Swanson EA, Lin CP, et al. Optical coherence tomography. *Science*. 1991;254:1178–1181
2. Hee MR, Izatt JA, Swanson EA, et al. Optical coherence tomography of the human retina. *Arch Ophthalmol*. 1995;113:325–332
3. Tsunoda K, Oguchi Y, Hanazono G, Tanifuji M. Mapping cone- and rod-induced retinal responsiveness in macaque retina by optical imaging. *Invest Ophthalmol Vis Sci*. 2004;45:3820–3826.

4. DeLint PJ, Berendschot TT, van de Kraats J, van Norren D. Slow optical changes in human photoreceptors induced by light. *Invest Ophthalmol Vis Sci.* 2000;41:282–289.
5. Nelson DA, Krupsky S, Pollack A, et al. Special report: Noninvasive multi-parameter functional optical imaging of the eye. *Ophthalmic Surg Lasers Imaging.* 2005;36:57–66.
6. Abramoff MD, Kwon YH, Ts'o D, et al. Visual stimulus-induced changes in human near-infrared fundus reflectance. *Invest Ophthalmol Vis Sci.* 2006;47:715–721.
7. Crittin M, Riva CE. Functional imaging of the human papilla and peripapillary region based on flicker-induced reflectance changes. *Neurosci Lett.* 2004;360:141–144.
8. Frostig RD, Lieke EE, Ts'o DY, Grinvald A. Cortical functional architecture and local coupling between neuronal activity and the microcirculation revealed by in vivo high-resolution optical imaging of intrinsic signals. *Proc Natl Acad Sci USA.* 1990;87:6082–6086.
9. Malonek D, Grinvald A. Interactions between electrical activity and cortical microcirculation revealed by imaging spectroscopy: implications for functional brain mapping. *Science.* 1996;272:551–554.
10. Tsunoda K, Yamane Y, Nishizaki M, Tanifuji M. Complex objects are represented in macaque inferotemporal cortex by the combination of feature columns. *Nat Neurosci.* 2001;4:832–838.
11. Pouratian N, Toga A. Optical imaging based on intrinsic signals. In: Toga AW, Mazziotta JC, eds. *Brain Mapping.* San Diego, CA: Academic Press; 2002:97–140.
12. Bowmaker JK, Dartnall HJ, Mollon JD. Microspectrophotometric demonstration of four classes of photoreceptor in an old world primate, Macaca fascicularis. *J Physiol.* 1980;298:131–143.
13. Bowmaker JK, Dartnall HJ. Visual pigments of rods and cones in a human retina. *J Physiol.* 1980;298:501–511.
14. Kilbride PE, Read JS, Fishman GA, Fishman M. Determination of human cone pigment density difference spectra in spatially resolved regions of the fovea. *Vision Res.* 1983;23:1341–1350.
15. Kilbride PE, Alexander KR, Fishman M, Fishman GA. Human macular pigment assessed by imaging fundus reflectometry. *Vision Res.* 1989;29:663–674.
16. Elsner AE, Burns SA, Webb RH. Mapping cone photopigment optical density. *J Opt Soc Am A.* 1993;10:52–58.
17. Wali N, Leguire LE. The photopic hill: a new phenomenon of the light adapted electroretinogram. *Doc Ophthalmol.* 1992;80:335–345.
18. Weinhaus RS, Burke JM, Delori FC, Snodderly DM. Comparison of fluorescein angiography with microvascular anatomy of macaque retinas. *Exp Eye Res.* 1995;61:1–16.
19. Fulton AB, Rushton WA. The human rod ERG: correlation with psychophysical responses in light and dark adaptation. *Vision Res.* 1978;18:793–800.
20. Wagman IH, Waldman J, Nakloff D, Feinschil LB, Cahan R. The recording of the electroretinogram in humans and in animals: investigation of retinal sensitivity following brief flashes of light. *Am J Ophthalmol.* 1954;38:60–69.
21. Mahroo OA, Lamb TD. Recovery of the human photopic electroretinogram after bleaching exposures: estimation of pigment regeneration kinetics. *J Physiol.* 2004;554:417–437.
22. Biersdorf WR, Armington JC. Level of light adaption and the human electroretinogram. *J Opt Soc Am.* 1960;50:78–82.
23. Bui BV, Fortune B. Origin of electroretinogram amplitude growth during light adaptation in pigmented rats. *Vis Neurosci.* 2006;23:155–167.
24. Miyake Y, Horiguchi M, Tomita N, et al. Occult macular dystrophy. *Am J Ophthalmol.* 1996;122:644–653.
25. Miyake Y, Shiroyama N, Horiguchi M, Ota I. Asymmetry of focal ERG in human macular region. *Invest Ophthalmol Vis Sci.* 1989;30:1743–1749.
26. Fukuda M, Rajagopalan UM, Homma R, Matsumoto M, Nishizaki M, Tanifuji M. Localization of activity-dependent changes in blood volume to submillimeter-scale functional domains in cat visual cortex. *Cereb Cortex.* 2005;15:823–833.
27. Riva CE, Harino S, Shonat RD, Petrig BL. Flicker evoked increase in optic nerve head blood flow in anesthetized cats. *Neurosci Lett.* 1991;128:291–296.
28. Riva CE, Falsini B, Logean E. Flicker-evoked responses of human optic nerve head blood flow: luminance versus chromatic modulation. *Invest Ophthalmol Vis Sci.* 2001;42:756–762.
29. Narayan SM, Esfahani P, Blood AJ, Sikkens L, Toga AW. Functional increases in cerebral blood volume over somatosensory cortex. *J Cereb Blood Flow Metab.* 1995;15:754–766.
30. Ransom BR, Yamate CL, Connors BW. Activity-dependent shrinkage of extracellular space in rat optic nerve: a developmental study. *J Neurosci.* 1985;5:532–535.
31. MacVicar BA, Feighan D, Brown A, Ransom B. Intrinsic optical signals in the rat optic nerve: role for K(+) uptake via NKCC1 and swelling of astrocytes. *Glia.* 2002;37:114–123.
32. Roy C, Sherrington C. On the regulation of the blood supply of the brain. *J Physiol.* 1890;11:85–108.
33. Villringer A, Dirnagl U. Coupling of brain activity and cerebral blood flow: basis of functional neuroimaging. *Cerebrovasc Brain Metab Rev.* 1995;7:240–276.
34. Yao XC, Yamauchi A, Perry B, George JS. Rapid optical coherence tomography and recording functional scattering changes from activated frog retina. *Appl Opt.* 2005;44:2019–2023.
35. Bizheva K, Pflug R, Hermann B, et al. Optophysiology: depth-resolved probing of retinal physiology with functional ultrahigh-resolution optical coherence tomography. *Proc Natl Acad Sci USA.* 2006;103:5066–5071.
36. Toth LJ, Rao SC, Kim DS, Somers D, Sur M. Subthreshold facilitation and suppression in primary visual cortex revealed by intrinsic signal imaging. *Proc Natl Acad Sci USA.* 1996;93:9869–9874.
37. Kaplan E, Benardete E. The dynamics of primate retinal ganglion cells. *Prog Brain Res.* 2001;134:17–34.
38. Maheswari RU, Takaoka H, Kadono H, Homma R, Tanifuji M. Novel functional imaging technique from brain surface with optical coherence tomography enabling visualization of depth resolved functional structure in vivo. *J Neurosci Methods.* 2003;124:83–92.
39. Srinivasan VJ, Wojtkowski M, Fujimoto JG, Duker JS. In vivo measurement of retinal physiology with high-speed ultrahigh-resolution optical coherence tomography. *Opt Lett.* 2006;31:2308–2310.

Graefe's Arch Clin Exp Ophthalmol
(2006) 244: 259–261

CASE REPORT

DOI 10.1007/s00417-005-0044-1

Yumi Suzuki
Eriko Kawase
Sachiko Nishina
Noriyuki Azuma

# Two patients with different features of congenital optic disc anomalies in the two eyes

Received: 23 January 2005
Revised: 21 April 2005
Accepted: 1 May 2005
Published online: 15 July 2005


Y. Suzuki · E. Kawase · S. Nishina · N. Azuma (✉)
Department of Ophthalmology,
National Center for Child Health and Development, 2-10-1,
Okura, Setagaya-ku,
Tokyo, 157-8535, Japan
e-mail: azuma-n@ncchd.go.jp
Tel.: +81-3-34160181
Fax: +81-3-34162222

**Abstract** *Purpose:* Description of two patients, each with different features of congenital optic disc anomalies in the two eyes. *Methods:* Case report *Results:* Patient 1, a 3-month-old girl, showed retinochoroidal coloboma involving the optic nerve in the right eye and optic nerve hypoplasia in the left eye. Patient 2, a 5-month-old boy, showed retinal fold extending inferiorly in the right eye and optic disc coloboma in the left eye. *Conclusions:* Since in both cases coloboma was seen in one eye, the optic nerve hypoplasia or retinal fold in the fellow eye of these two patients may have been related to the timing of embryonic fissure opening or closing.

**Keywords** Congenital optic disc anomalies · Coloboma · Optic nerve hypoplasia · Retinal fold

## Introduction

Numerous developmental events contribute to optic disc/nerve formation, including transient formation of embryonic fissure, hyaloid artery, and Bergmeister's papilla, and projection of nerve fibers. Thus, optic disc/nerve malformations occur when these developmental events transiently or spatially arrest and may present a variety of fundus features. Bilateral anomalies usually show the same phenotype, because of the same genetic background, intrauterine circumstances, or timing of a causative intervention. We report two patients with bilateral optic disc/nerve anomalies that were different clinical entities in the two eyes.

## Case report

Patient 1, a 3-month-old girl, presented with nystagmus in both eyes. Ocular examinations showed normal anterior segments, large retinochoroidal coloboma involving the optic nerve in the right eye, and hypoplasia of the optic nerve with a small optic disc and surrounding depigmented ring (double-ring sign) in the left eye. Computed tomography (CT) identified hypoplasia of the cerebellar vermis, a callosal defect, ventricular enlargement, and extrusion of the posterior portion of the eyeball in the right eye and a thin optic nerve in the left eye (Fig. 1). The patient, now 3 years old and mentally challenged, has normal growth and no systemic abnormalities.

Patient 2, a 5-month-old boy, presented with nystagmus in both eyes. A retinal fold was seen extending from the optic disc and connected to fibrous tissue on the inferior portion of the posterior lens surface in the right eye. The left anterior segment was normal, although the fundus had a classic optic disc coloboma (Fig. 2). CT was normal, except for the retinal fold in the right eye and eye wall ectasia of the optic nerve region in the left eye. The patient, now 7 years old and mentally challenged, has normal growth and no systemic abnormalities. Other family members of each patient were apparently normal, thus indicating sporadic onset. Each patient was the product of a full-term pregnancy, and careful pediatric examination failed to identify any history of infectious disease.

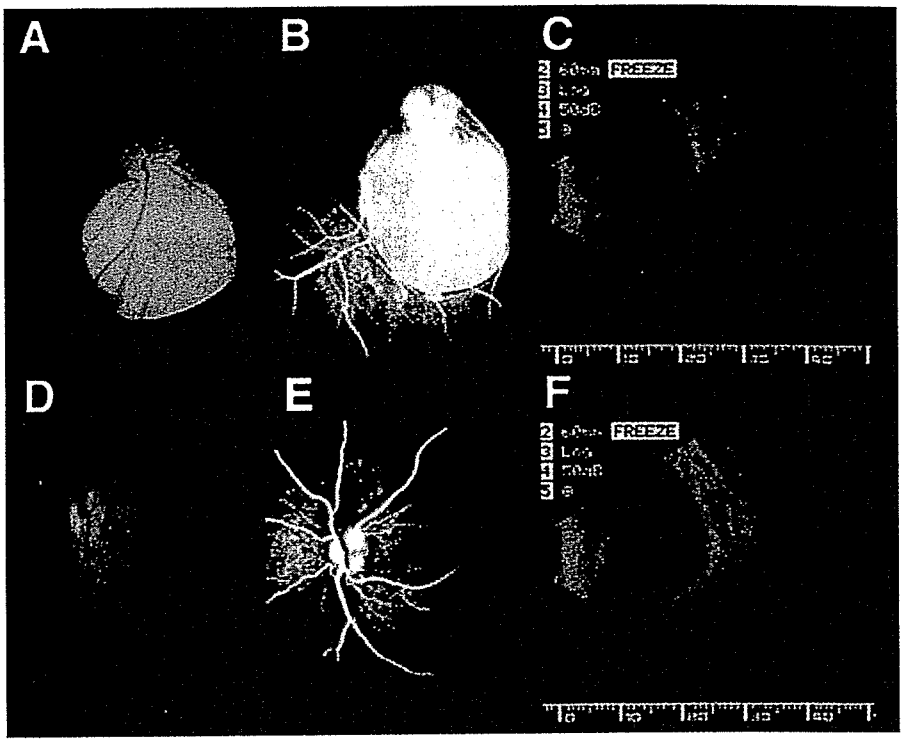


**Fig. 1** Fundus photography (**a**, **d**), fluorescein angiography (**b**, **e**), and echography (**c**, **f**) of patient 1 show large retinochoroidal coloboma that involves the optic disc OD (**a**–**c**) and optic hypoplasia OS (**d**–**f**)

## Discussion

Among events related to optic disc/nerve formation, opening and closing of the embryonic fissure at 5–6 weeks gestation, when transiently arrested, are the most common pathogenetic factors for malformations associated with peripapillary excavation, including coloboma, peripapillary staphyloma, and morning glory disc anomaly. Slightly different manifestations of optic disc/nerve anomalies (coloboma, optic disc pit) were reported bilaterally in the affected members of a pedigree showing inherited defects, suggesting that the difference depended on the degree of peripapillary excavation and that both anomalies are in the same spectrum [9].

In contrast, the fundus features in the two eyes of each of our patients markedly differed. Optic nerve hypoplasia is

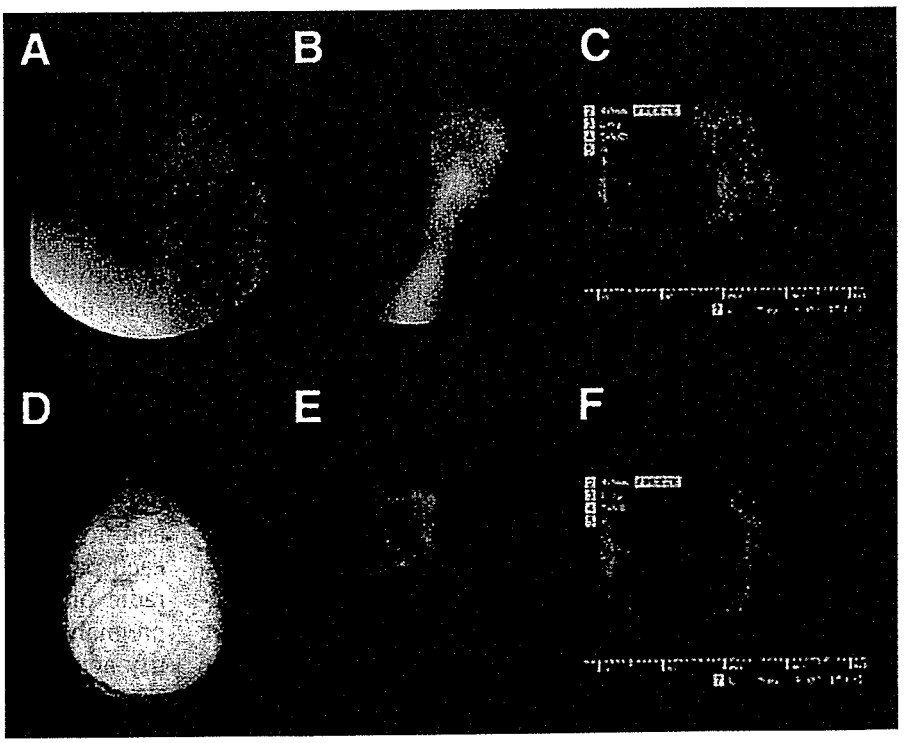


**Fig. 2** Fundus photography (**a**, **d**), fluorescein angiography (**b**, **e**), and echography (**c**, **f**) of patient 2 show fibrous tissue on the inferior retinal periphery and retinal fold OD (**a**–**c**) and coloboma that involves the optic disc OS (**d**–**f**)